Nonmonotonic behaviors of Fano factor in double quantum dot connected with Luttinger liquid electrodes



2009 J. Phys.: Condens. Matter 21 395303

(http://iopscience.iop.org/0953-8984/21/39/395303)

J. Phys.: Condens. Matter **21** (2009) 395303 (16pp) doi:10.1088/0953-8984/21/39/395303

# Nonmonotonic behaviors of Fano factor in double quantum dot connected with Luttinger liquid electrodes

**Satoshi Kawaguchi**

Department of Complex Systems, School of Systems Information Science,
Future University-Hakodate, Hakodate 041-8655, Japan

Received 7 April 2009, in final form 8 July 2009
Published 8 September 2009
Online at stacks.iop.org/JPhysCM/21/395303

**Abstract**

In this study, we discuss the behavior of the Fano factor in a double quantum dot (DQD) connected with Luttinger liquid (LL) electrodes. At the Toulouse point, we study the dependence of the Fano factor on the bias voltage, the energy level of the dots, the interdot coupling, and the asymmetry parameter. We show that the behavior of the Fano factor in a DQD is similar to that in a single quantum dot (SQD); however, it behaves nonmonotonically with bias voltage and three local extrema can occur. The condition for the occurrence of nonmonotonic behavior is determined, and it is shown that local extrema result from the mixing of the bare energy levels of the dots caused by the interdot coupling. The influence of the Klein factor on the conductance in a DQD and the limitation of the perturbation calculation for a DQD are discussed.

## 1. Introduction

Recent developments in fabrication techniques has made it possible to fabricate nanoscale devices such as quantum dots and one-dimensional quantum wires. Single-walled carbon nanotubes (SWNTs) are promising candidates for the fabrication of one-dimensional quantum wires. The noteworthy feature of this one-dimensional electron system is that it is not described by a Fermi liquid, but by the Luttinger liquid (LL). In a LL, physical observables scale as power laws with respect to external parameters such as bias voltage and temperature [1, 2]. Experiments on carbon nanotubes have shown that the conductance and differential conductance obey a power law [3]. Several experiments have been carried out to study the conductance and its temperature dependence in quantum wires, SQDs, and/or DQDs in carbon nanotubes [4–8].

Recently, not only the current but also the current correlation have attracted considerable attention from researchers. As compared to the average current, the current correlation, measured as current noise, provides considerable information about quantum transport. The current noise originates from the fluctuation of the current from its average value. The Fourier transform of the current noise gives the noise power. In the zero-frequency limit, current noise consists of thermal noise (Johnson–Nyquist noise) and shot noise [9]. The shot noise in noninteracting systems is suppressed below the Poisson noise $2eI$, where $e$ is the elementary electron charge and $I$ is the average current. In order to characterize the deviation from the Poisson noise, the Fano factor is often used, which is defined as the ratio between the shot noise and the Poisson noise. Due to the difficulty involved in device preparation and the detection of weak excess noise against the prevalent background noise, there are few experiments on the shot noise in carbon nanotubes [10, 11]. The experimental results exhibit that the shot noise and the Fano factor scale as a power law with the bias voltage. Super-Poissonian noise is detected in the Coulomb diamond, which results from the inelastic cotunneling.

For the theoretical point of view, many studies have been conducted on the transport properties of a quantum dot connected with LL electrodes [12–16]. The Coulomb interaction and the charging effect in quantum dots play important roles. The conductance peak is governed by power law scaling. Recently, the shot noise properties of an inhomogeneous LL model and a Coulomb blockade region were studied [17–21]. When sequential tunneling is dominant, the Fano factor is sub-Poissonian. In contrast, in the Coulomb blockade region, the cotunneling process is dominant. In such a case, the Fano factor becomes either Poissonian or super-Poissonian, depending on the ground state of the nanotube.

In this paper, we study a DQD connected with LL electrodes and examine the properties of the shot noise.

 

We consider the case in which the intradot and interdot Coulomb interactions are neglected, but where the electrostatic Coulomb interaction between dots and electrodes is taken into consideration. Although the intradot and interdot Coulomb interactions may play important roles in electron conduction, the electron correlation in DQDs is not taken into consideration so that our results are valid at temperatures higher than the Kondo temperature. The strong LL correlation in SWNTs is observed over a wide range of temperatures, which are considerably higher than the Kondo temperature [3, 6]. This supports our idea of neglecting the intradot and interdot Coulomb interactions in the model. The analysis of the model Hamiltonian is difficult for the general strength of the Coulomb interaction. However, using bosonization and refermionization methods, the Hamiltonian is mapped to a Kondo-type model. This system can be solved exactly for a particular strength of the Coulomb interaction, the Toulouse point [22]. The Toulouse approach was first applied to a two-channel Kondo model at a particular strength of the longitudinal exchange coupling, the model was mapped to an exactly solvable resonant-level model [23]. The method was extended to the nonequilibrium Kondo model, and current, noise spectra, and magnetic properties were studied [24]. Recently, the full counting statistics for a Kondo dot at the Toulouse point was studied [25–27].

The electron tunneling between multiple LL electrodes via the resonant level in a SQD was studied by using the renormalization group method [28]. It was shown that there is a stable fixed point at an intermediate coupling strength when the LL parameter $g$ is in the range $1/3 < g < 9$. From this point of view, the study on the conductance in a SQD connected with two LL electrodes at the Toulouse point with $g = 1/2$ is justified [29]. In [29], the exact transmission probability is obtained by using the equation of motion method, and it is shown that the shot noise is sub-Poissonian, and the Fano factor behaves nonmonotonically with bias voltage when the coupling is asymmetric or the energy level of a dot is out of resonance. It is known that strong Coulomb correlations in a DQD cause the nonmonotonic behavior of the Fano factor [30–32]. In contrast, although the intradot and interdot Coulomb interactions were not considered in [29], the Fano factor showed a nonmonotonic behavior with bias voltage.

The conductance in a SQD with two states, and quantum rachet effects were studied in [29]. However, the properties of the shot noise in a DQD connected with LL electrodes have not been studied thus far. In this study, we extend the model Hamiltonian for a SQD given in [29] to a DQD. We first verify the validity of the perturbation method for a SQD and study the mechanism and condition of the nonmonotonic behavior of the Fano factor. Second, we discuss how the Fano factor is influenced by the energy levels of dots, interdot coupling, and the asymmetry parameter in a DQD. We also discuss the influence of the Klein factor and the limitation of the perturbation expansion for a DQD.

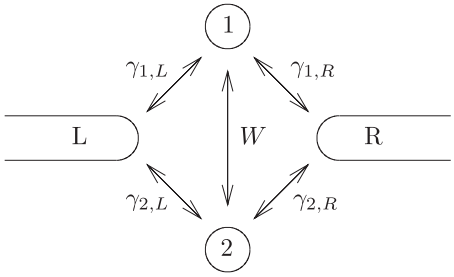


**Figure 1.** Double quantum dot connected with LL electrodes. For a serial DQD, $\gamma_{1,\mathrm{L}} = \gamma_{2,\mathrm{R}} = 0$; for a T-shaped DQD, $\gamma_{2,\mathrm{L}} = \gamma_{2,\mathrm{R}} = 0$; and for a parallel DQD, $\gamma_{1(2),\mathrm{L(R)}} \neq 0$.

## 2. Model and method

We first introduce the model Hamiltonian and derive the current and noise formulae for a general configuration of a DQD system by $S$-matrix expansion. In order to calculate the current and the shot noise, it is necessary to determine Green's functions. We derive the complete set of Green's functions by perturbation expansion up to the second order of tunneling amplitudes between dots and leads.

### *2.1. Model Hamiltonian*

We consider DQD systems connected with semi-infinite LL electrodes. There are three types of DQD systems: serial, T-shaped, and parallel. The geometry of the systems is shown in figure 1. A DQD is placed at $x = 0$, where the left- and right-hand side electrodes are connected. The Hamiltonian of this system is given by the sum of three parts:

$$H = H_{\mathrm{K}} + H_{\mathrm{t}} + H_{\mathrm{C}}, \tag{2.1}$$

where

$$H_{\mathrm{K}} = H_{\mathrm{lead}}[\psi_{\mathrm{L}}, \psi_{\mathrm{R}}] + \sum_{i=1,2} \Delta_i d_i^\dagger d_i + W(d_1^\dagger d_2 + \mathrm{h.c.}), \tag{2.2}$$

$$H_{\mathrm{t}} = \sum_{i=1,2} \sum_{j=\mathrm{R,L}} \gamma_{i,j}(d_i^\dagger \psi_j(0) + \mathrm{h.c.}), \tag{2.3}$$

and

$$H_{\mathrm{C}} = \lambda_{\mathrm{C}} \sum_{i=1,2} d_i^\dagger d_i \sum_{j=\mathrm{R,L}} \psi_j^\dagger(0)\psi_j(0). \tag{2.4}$$

Here, $H_{\mathrm{K}}$ is a kinetic part, and $H_{\mathrm{lead}}$ describes the electrons in the leads; the chemical potential difference between the left- and right-hand side leads is fixed as $\mu_{\mathrm{L}} - \mu_{\mathrm{R}} = eV$. The bias voltage is symmetrically applied. We consider spinless electrons. Let $d_i$ and $\Delta_i$ denote the annihilation operator and the energy level of dot $i$ ($i = 1$ and 2), respectively, and $W$ denote the amplitude of the interdot coupling. We assume that the chemical potentials of the left- and right-hand side leads without bias voltage are $\mu_{\mathrm{L}} = \mu_{\mathrm{R}} = \mu$. The energy level $\Delta_i$ is measured relative to $\mu$. $H_{\mathrm{t}}$ denotes the tunnel coupling between the dot $i$ and the lead $j$ ($j =$ L and R), which occurs at $x = 0$, with amplitudes $\gamma_{i,j}$. $H_{\mathrm{C}}$ denotes the electrostatic Coulomb interaction between electrons at $x = 0$ in both leads and dots. In this study, although the short-ranged (screened)

Coulomb interaction between electrons in leads is considered, the intradot and interdot Coulomb interactions are not taken into consideration.

$H_{\rm lead}$ is given as

$$H_{\rm lead}[\psi_{\rm L},\psi_{\rm R}] = {\rm i}\hbar v_{\rm F}\sum_{j={\rm L,R}}\int {\rm d}x\ \psi_j^\dagger(x)\partial_x\psi_j(x) + \frac{1}{2}\int {\rm d}x\ U_{\rm c}\sum_j \rho_j^2(x) + \frac{eV}{2}\int {\rm d}x\ (\rho_{\rm L}(x)-\rho_{\rm R}(x)) \equiv H_0 + H_{\rm I} + H_{\rm b}, \tag{2.5}$$

where $v_{\rm F}$ is the Fermi velocity, $H_{\rm I}$ denotes the short-ranged Coulomb interaction in the leads, $U_{\rm c}$ is the bare Coulomb interaction strength, and $\rho_j(x)$ is the density operator in lead $j$, which is given by $\rho_j = :\psi_j^\dagger(x)\psi_j(x):$, where the fermion fields $\psi_j$ are normal ordered [33]. An electron system composed of two semi-infinite leads is described by the chiral fermions in an infinite lead with the negative half-axis representing the particles moving toward $x = 0$, and the positive half-axis representing the particles moving away from $x = 0$ [34]. In the bosonic representation, the part $(H_0 + H_{\rm I})$ can be simply described in the form of the noninteracting electron system by the renormalizations of the boson fields and the Fermi velocity by the LL parameter $g$, given by $g = (1 + U_{\rm c}/\pi\hbar v_{\rm F})^{-1/2}$. For repulsive interactions, $g < 1$ [35].

The electron field $\psi_j(x)$ is expressed in terms of the bosonic field $\phi_j(x)$ by

$$\psi_j(x) = \frac{1}{\sqrt{2\pi a_0}}F_{\eta_j}{\rm e}^{{\rm i}\phi_j(x)/\sqrt{g}}, \tag{2.6}$$

where $a_0$ is a lattice constant, and $F_{\eta_j}$ is the Klein factor, which satisfies $\{F_{\eta_k}, F_{\eta_l}\}_+ = 2\delta_{kl}$ and $F_{\eta_k}^\dagger = F_{\eta_k}$, (where $k$ and $l$ are either L or R). This ensures the anticommutation relation between $\psi_k$ and $\psi_l^\dagger$. Using this bosonic representation, $(H_0 + H_{\rm I})$ is described by $H_{\rm LL}$ as

$$H_{\rm LL} = \frac{1}{4\pi}\left(\frac{v_{\rm F}}{g}\right)\sum_j\int {\rm d}x\ [\partial_x\phi_j(x)]^2. \tag{2.7}$$

In the bosonic representation [36], the relation between the density operator $\rho_j$ and the phase field $\phi_j(x)$ is given as

$$\rho_j(x) = \partial_x\phi_j(x)/2\pi\sqrt{g}. \tag{2.8}$$

The electron field at the boundary $x = 0$ is given by

$$\psi_j(0) = \frac{1}{\sqrt{2\pi a_0}}F_{\eta_j}{\rm e}^{{\rm i}\phi_j(0)/\sqrt{g}}. \tag{2.9}$$

In order to solve the Hamiltonian (2.1), we first transform $d_i^\dagger$ and $d_i$ to a spin representation of the form [22]

$$S_i^x = (d_i^\dagger + d_i)/2, \qquad S_i^y = -{\rm i}(d_i^\dagger - d_i)/2, \qquad S_i^z = (d_i^\dagger d_i - 1/2). \tag{2.10}$$

From this spin representation, it is found that $H_{\rm C}$ is equivalent to the $S_z$ spin-density coupling term in the Kondo Hamiltonian. In order to solve the Hamiltonian, we apply the transformation. We first define the symmetric and antisymmetric fields as

$$\phi_\pm = (\phi_{\rm L} \pm \phi_{\rm R})/\sqrt{2}, \tag{2.11}$$

where $\phi_\pm$ satisfy the bosonic commutation relations. Similar to Emery and Kivelson's study [23], we apply the canonical transformation $H' = U^\dagger H U$ with

$$U = \exp\left({\rm i}\sum_{i=1,2} S_i^z\phi_+(0)/\sqrt{2g}\right). \tag{2.12}$$

The transformed Hamiltonians are

$$H'_{\rm K} + H'_{\rm C} = H_{\rm K} + \sum_i\left(\lambda_{\rm C}/\pi\sqrt{2g} - \hbar\left(\frac{v_{\rm F}}{g}\right)\sqrt{2/g}\right) \times S_i^z\partial_x\phi_+(0), \tag{2.13}$$

and

$$H'_{\rm t} = (2\pi a_0)^{-1/2}\sum_i[S_i^+(\gamma_{i,{\rm L}}F_{\eta_{\rm L}}{\rm e}^{{\rm i}\phi_-/\sqrt{2g}} + \gamma_{i,{\rm R}}F_{\eta_{\rm R}}{\rm e}^{-{\rm i}\phi_-/\sqrt{2g}}) + (\gamma_{i,{\rm L}}F_{\eta_{\rm L}}{\rm e}^{-{\rm i}\phi_-/\sqrt{2g}} + \gamma_{i,{\rm R}}F_{\eta_{\rm R}}{\rm e}^{{\rm i}\phi_-/\sqrt{2g}})S_i^-]_{x=0}, \tag{2.14}$$

where $S_i^\pm = S_i^x \pm {\rm i}S_i^y = d_i^\dagger, d_i$. Neglecting the Klein factor $F_{\eta_{\rm L(R)}}$, at the point $g = 1/2$, we can refermionize the problems by using new fermion fields

$$\psi_\pm = {\rm e}^{{\rm i}\phi_\pm}/\sqrt{2\pi a_0}, \tag{2.15}$$

where $\psi_\pm$ satisfy fermionic commutation relations, and the Klein factor $F_{\eta_\pm}$ is neglected. Using the particle density operator $\psi_\pm^\dagger\psi_\pm = \partial_x\phi_\pm/2\pi$, the refermionized Hamiltonian takes the form

$$H = H_{\rm lead}[\psi_\pm] + \sum_{i=1,2}[(\lambda_{\rm C} - 2\pi\hbar v'_{\rm F})2S_i^z\psi_+^\dagger\psi_+ + \Delta_i S_i^z + S_i^+(\gamma_{i,{\rm L}}\psi_- + \gamma_{i,{\rm R}}\psi_-^\dagger) + (\gamma_{i,{\rm L}}\psi_-^\dagger + \gamma_{i,{\rm R}}\psi_-)S_i^-]_{x=0} + W(d_1^\dagger d_2 + {\rm h.c.}), \tag{2.16}$$

where the scaled Fermi velocity $v'_{\rm F} = (v_{\rm F}/g)$ and

$$H_{\rm lead}[\psi_\pm] = {\rm i}\hbar v'_{\rm F}\sum_{j=\pm}\int {\rm d}x\ \psi_j^\dagger\partial_x\psi_j + eV\int {\rm d}x\ \psi_-^\dagger\psi_-. \tag{2.17}$$

It is noted that equation (2.16) has a similar form to the Kondo model, and the $\pm$ channels are decoupled at the Toulouse point when $\lambda_{\rm C} = 2\pi\hbar v'_{\rm F}$. It has been shown that this Kondo model in nonequilibrium is exactly solvable at the Toulouse point [24]. We discuss properties at the Toulouse point, where the + channel is free, so that we do not have to consider this channel in the following discussions. In order to calculate the current and the shot noise, we apply the perturbation expansion in terms of small $\gamma_{i,j}$. We first introduce the real (Majorana) fermions $a_i$, $b_i$, $\zeta$, and $\eta$:

$$d_i = (a_i + {\rm i}b_i)/\sqrt{2}, \qquad \psi_- = (\zeta + {\rm i}\eta)/\sqrt{2}, \tag{2.18}$$

where $a_i$, $b_i$, $\zeta$, and $\eta$ satisfy $a_i^2 = b_i^2 = \zeta^2 = \eta^2 = \frac{1}{2}$. Using these Majorana fermions, the Hamiltonian is written as

$$H = H_0 + H_1, \tag{2.19}$$

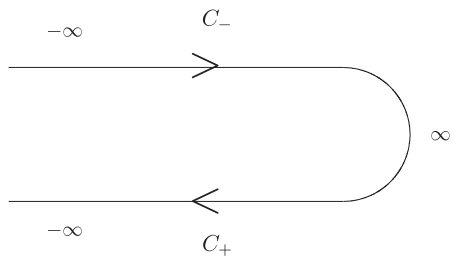


**Figure 2.** Complex-time contour for which nonequilibrium Green's functions are defined.

where the unperturbed part

$$H_0[\zeta,\eta;a_1,b_1,a_2,b_2] = \mathrm{i}\int \mathrm{d}x\,[\hbar v'_{\mathrm{F}}(\zeta(x)\partial_x\zeta(x) + \eta(x)\partial_x\eta(x)) + eV\zeta(x)\eta(x)] + \mathrm{i}(\Delta_1 a_1 b_1 + \Delta_2 a_2 b_2 + W a_1 b_2 + W a_2 b_1) \tag{2.20}$$

and the perturbed part

$$H_1 = -\mathrm{i}(\gamma_{+1}b_1\zeta(0) + \gamma_{-1}a_1\eta(0) + \gamma_{+2}b_2\zeta(0) + \gamma_{-2}a_2\eta(0)). \tag{2.21}$$

Here, for convenience, we changed the tunnel amplitude from $\gamma_{i,j}$ to $\gamma_{\pm i}$ defined by

$$\gamma_{\pm i} = \gamma_{i,\mathrm{L}} \pm \gamma_{i,\mathrm{R}}. \tag{2.22}$$

In chiral formulations, the bias voltage leads to a difference in the densities of the incoming particles in both channels [34]. The current is proportional to the difference between the densities of the incoming and outgoing particles in each channel, $J = -ev_{\mathrm{F}}(\rho_{\mathrm{L}} - \rho_{\mathrm{R}})$. Applying the canonical transformation (2.12) to $J$, we set $N_- = \psi_-^\dagger\psi_-$. The current operator in terms of the Majorana fermions is defined by

$$J = -e\frac{\mathrm{d}N_-}{\mathrm{d}t} = \frac{-\mathrm{i}e}{\hbar}(\gamma_{-1}a_1\zeta(0) + \gamma_{+1}b_1\eta(0) + \gamma_{-2}a_2\zeta(0) + \gamma_{+2}b_2\eta(0)). \tag{2.23}$$

Using the perturbed part $H_1$ of the Hamiltonian, the $S$ matrix is defined by

$$S = T_C\exp\Big[-\int_C \mathrm{d}\tau\,(\gamma_{+1}b_1(\tau)\zeta(\tau) + \gamma_{-1}a_1(\tau)\eta(\tau) + \gamma_{+2}b_2(\tau)\zeta(\tau) + \gamma_{-2}a_2(\tau)\eta(\tau))\Big], \tag{2.24}$$

where $T_{\mathrm{C}}$ is the time-ordering operator along the Keldysh contour $C$, as shown in figure 2, which consists of the forward $C_-$ and the backward $C_+$ paths. The averages are calculated by using the $S$ matrix as $\langle\cdots\rangle = \langle\cdots S\rangle_0$.

### 2.2. Current and noise

In order to consider the nonequilibrium state of the system, we define Green's functions for the Majorana fermions as

$$\begin{aligned} D^{ij}_{fh}(t,t') &= -\mathrm{i}\langle T_C f(t)h(t')\rangle,\\ G^{ij}_{\mu\nu}(t,t') &= -\mathrm{i}\langle T_C \mu(t)\nu(t')\rangle,\\ G^{ij}_{\mu f}(t,t') &= -\mathrm{i}\langle T_C \mu(t)f(t')\rangle,\\ G^{ij}_{f\mu}(t,t') &= -\mathrm{i}\langle T_C f(t)\mu(t')\rangle, \end{aligned} \tag{2.25}$$

where $f$ and $h$ indicate either $a_{1,2}$ or $b_{1,2}$, and $\mu$ and $\nu$ indicate either $\zeta$ or $\eta$. The times $t$ and $t'$ pertain to the paths $C_i$ and $C_j$, respectively, where $i$ and $j$ indicate either $+$ or $-$. Using the abovementioned Green's functions, we define advanced and retarded Green's functions as $G^{\mathrm{a}} = G^{--} - G^{+-} = -G^{++} + G^{-+}$ and $G^{\mathrm{r}} = G^{--} - G^{-+} = -G^{++} + G^{+-}$, respectively. In the steady state, Green's functions are translationally invariant in the time domain; they depend on the time difference $(t - t')$. Therefore, we can define their Fourier transformation.

Assuming that $\gamma_\pm$ are small, we expand the $S$ matrix in terms of $\gamma_\pm$. To simplify the calculations, we set $v'_{\mathrm{F}} = 1$. By applying the equation of motion method to the unperturbed Hamiltonian (2.20), we can obtain zero order Green's functions. Putting $\gamma_{\pm1} = \gamma_{\pm2} = 0$, the zero order Green's functions of the $\zeta$–$\eta$ subsystems are obtained as

$$G^{(0)ij}_{\zeta\zeta}(\omega) = G^{(0)ij}_{\eta\eta}(\omega) = \frac{\mathrm{i}}{2}\begin{pmatrix} H(\omega) & H(\omega)+1 \\ H(\omega)-1 & H(\omega)\end{pmatrix},$$
$$G^{(0)ij}_{\zeta\eta}(\omega) = -G^{(0)ij}_{\eta\zeta}(\omega) = \tfrac{1}{2}F(\omega)\begin{pmatrix} 1 & 1 \\ 1 & 1\end{pmatrix}, \tag{2.26}$$

where the Fermi distribution function $n_{\mathrm{F}}(\omega) = \frac{1}{\mathrm{e}^{\omega\beta}+1}$, $H(\omega) = n_{\mathrm{F}}(\omega + eV) - n_{\mathrm{F}}(-\omega + eV)$, and $F(\omega) = n_{\mathrm{F}}(\omega + eV) - n_{\mathrm{F}}(\omega - eV)$. From equations (2.26), the retarded and advanced Green's functions are $G^{(0)\mathrm{r},(\mathrm{a})}_{\mu\nu} = 0$ and $G^{(0)\mathrm{r},(\mathrm{a})}_{\mu\mu} = \mp\mathrm{i}/2$, respectively.

The zero order Green's functions of the $a$–$b$ subsystem are obtained similarly. The time-ordered and antitime-ordered Green's functions are

$$\begin{aligned} D^{(0)--(++)}_{a_1a_1} &= D^{(0)--(++)}_{b_1b_1} = \pm\frac{1}{D}[\omega(\omega^2 - \Delta_2^2 - W^2)],\\ D^{(0)--(++)}_{a_2a_2} &= D^{(0)--(++)}_{b_2b_2} = \pm\frac{1}{D}[\omega(\omega^2 - \Delta_1^2 - W^2)],\\ D^{(0)--(++)}_{a_1a_2} &= D^{(0)--(++)}_{a_2a_1} = D^{(0)--(++)}_{b_1b_2}\\ &= D^{(0)--(++)}_{b_2b_1} = \pm\frac{1}{D}[\omega W(\Delta_1 + \Delta_2)],\\ D^{(0)--(++)}_{a_1b_1} &= -D^{(0)--(++)}_{b_1a_1} = \pm\frac{\mathrm{i}}{D}[\Delta_1(\omega^2 - \Delta_2^2) + W^2\Delta_2],\\ D^{(0)--(++)}_{a_2b_2} &= -D^{(0)--(++)}_{b_2a_2} = \pm\frac{\mathrm{i}}{D}[\Delta_2(\omega^2 - \Delta_1^2) + W^2\Delta_1],\\ D^{(0)--(++)}_{a_1b_2} &= D^{(0)--(++)}_{a_2b_1} = -D^{(0)--(++)}_{b_2a_1}\\ &= -D^{(0)--(++)}_{b_1a_2} = \pm\frac{\mathrm{i}}{D}[W(\omega^2 + \Delta_1\Delta_2 - W^2)], \end{aligned} \tag{2.27}$$

where $D(\omega) = \Pi_{p=\pm}[\Pi_i(\omega + p\Delta_i) - W^2]$, and the antitime-ordered Green's function corresponds to the lower sign in the

right-hand side. The lesser and greater Green's functions are

$$
\begin{aligned}
&D^{(0)-+(+-)}_{a_1a_1} = D^{(0)-+(+-)}_{b_1b_1} = \pm \mathrm{i}\pi\delta(\omega+\lambda_1),\\
&D^{(0)-+(+-)}_{a_2a_2} = D^{(0)-+(+-)}_{b_2b_2} = \pm \mathrm{i}\pi\delta(\omega+\lambda_2),\\
&D^{(0)-+(+-)}_{a_1a_2} = D^{(0)-+(+-)}_{b_1b_2}\\
&\quad = \pm \mathrm{i}\frac{(\Delta_1-\Delta_2)-\sqrt{(\Delta_1-\Delta_2)^2+4W^2}}{2W}\pi\delta(\omega+\lambda_2),\\
&D^{(0)-+(+-)}_{a_2a_1} = D^{(0)-+(+-)}_{b_2b_1}\\
&\quad = \mp \mathrm{i}\frac{(\Delta_1-\Delta_2)-\sqrt{(\Delta_1-\Delta_2)^2+4W^2}}{2W}\pi\delta(\omega+\lambda_1),\\
&D^{(0)-+(+-)}_{a_1b_1} = -D^{(0)-+(+-)}_{b_1a_1} = \pm\pi\delta(\omega+\lambda_1),\\
&D^{(0)-+(+-)}_{a_2b_2} = -D^{(0)-+(+-)}_{b_2a_2} = \pm\pi\delta(\omega+\lambda_2),\\
&D^{(0)-+(+-)}_{a_1b_2} = -D^{(0)-+(+-)}_{b_1a_2}\\
&\quad = \pm\frac{(\Delta_1-\Delta_2)-\sqrt{(\Delta_1-\Delta_2)^2+4W^2}}{2W}\pi\delta(\omega+\lambda_2),\\
&D^{(0)-+(+-)}_{a_2b_1} = -D^{(0)-+(+-)}_{b_2a_1}\\
&\quad = \mp\frac{(\Delta_1-\Delta_2)-\sqrt{(\Delta_1-\Delta_2)^2+4W^2}}{2W}\pi\delta(\omega+\lambda_1),
\end{aligned}
\tag{2.28}
$$

where $\lambda_{1,2} = \frac{1}{2}[(\Delta_1+\Delta_2) \pm \sqrt{(\Delta_1-\Delta_2)^2+4W^2}]$, and the greater Green's function corresponds to the lower sign in the right-hand side. In order to prevent the divergence of equations (2.27), $D(\omega)$ in each denominator is replaced by $D(\omega) = \Pi_{p=\pm}\Pi_i(\omega + p\lambda_i + \mathrm{i}\delta)$ with an arbitrary positive small $\delta$.

The average current is obtained by expanding the $S$ matrix in terms of $\gamma_{\pm1,2}$. Up to the second order of $\gamma_{\pm1,2}$, the current is given in the form proposed by Meir and Wingreen [37] as

$$
\begin{aligned}
I(V) = \langle J\rangle = \frac{\mathrm{i}e}{\hbar}\frac{1}{2\pi}\int \mathrm{d}\omega\, \mathrm{Tr}[&G^{(0)}_{\zeta\eta}(-\omega)\\
&\times(\Gamma^{++}D^{\mathrm{a}}_{bb}(\omega) - \Gamma^{--}D^{\mathrm{a}}_{aa}(\omega))],
\end{aligned}
\tag{2.29}
$$

where

$$
\begin{aligned}
\Gamma^{\pm\pm} &= \begin{pmatrix} \gamma^2_{\pm1} & \gamma_{\pm1}\gamma_{\pm2} \\ \gamma_{\pm2}\gamma_{\pm1} & \gamma^2_{\pm2}\end{pmatrix},\\
D^{\mathrm{a}}_{fh} &= \begin{pmatrix} D^{\mathrm{a}}_{f_1h_1} & D^{\mathrm{a}}_{f_1h_2} \\ D^{\mathrm{a}}_{f_2h_1} & D^{\mathrm{a}}_{f_2h_2}\end{pmatrix},
\end{aligned}
\tag{2.30}
$$

where $f$ and $h$ are either $a$ or $b$.

The current noise is defined by the power spectrum of the current fluctuations. Using the current operator (2.23), we can derive the noise spectrum. It is divided into parallel and perpendicular components:

$$
\begin{aligned}
P(\Omega) &= \int \mathrm{d}t\, \mathrm{e}^{\mathrm{i}\Omega t}[\langle J(t)J(0)\rangle - \langle J(0)\rangle^2]\\
&\equiv P_{\parallel}(\Omega) + P_{\perp}(\Omega),
\end{aligned}
\tag{2.31}
$$

where

$$
\begin{aligned}
P_{\parallel}(\Omega) = \frac{1}{2\pi}\left(\frac{-\mathrm{i}e}{\hbar}\right)^2 \int \mathrm{d}\omega\, \mathrm{Tr}[&G^{+-}_{\zeta\zeta}(\Omega-\omega)\Gamma^{--}D^{+-}_{aa}(\omega)\\
&+ G^{+-}_{\eta\eta}(\Omega-\omega)\Gamma^{++}D^{+-}_{bb}(\omega)\\
&- \Gamma^{--}G^{+-}_{a\zeta;\zeta a}(\omega) - \Gamma^{++}G^{+-}_{b\eta;\eta b}(\omega)]
\end{aligned}
\tag{2.32}
$$

and

$$
\begin{aligned}
P_{\perp}(\Omega) = \frac{1}{2\pi}\left(\frac{-\mathrm{i}e}{\hbar}\right)^2 \int \mathrm{d}\omega\, \mathrm{Tr}[&G^{+-}_{\zeta\eta}(\Omega-\omega)\Gamma^{+-}D^{+-}_{ab}(\omega)\\
&+ G^{+-}_{\eta\zeta}(\Omega-\omega)\Gamma^{-+}D^{+-}_{ba}(\omega)\\
&- \Gamma^{+-}G^{+-}_{a\eta;\zeta b}(\omega) - \Gamma^{-+}G^{+-}_{b\zeta;\eta a}(\omega)],
\end{aligned}
\tag{2.33}
$$

where

$$
\begin{aligned}
\Gamma^{\pm\mp} &= \begin{pmatrix} \gamma_{\pm1}\gamma_{\mp1} & \gamma_{\pm1}\gamma_{\mp2} \\ \gamma_{\pm2}\gamma_{\mp1} & \gamma_{\pm2}\gamma_{\mp2}\end{pmatrix},\\
D^{+-}_{fh}(\omega) &= \begin{pmatrix} D^{+-}_{f_1h_1}(\omega) & D^{+-}_{f_1h_2}(\omega) \\ D^{+-}_{f_2h_1}(\omega) & D^{+-}_{f_2h_2}(\omega)\end{pmatrix},\\
G^{+-}_{f\mu;\nu h}(\omega) &= \begin{pmatrix} G^{+-}_{f_1\mu}(\omega)G^{+-}_{\nu h_1}(\Omega-\omega) & G^{+-}_{f_1\mu}(\omega)G^{+-}_{\nu h_2}(\Omega-\omega) \\ G^{+-}_{f_2\mu}(\omega)G^{+-}_{\nu h_1}(\Omega-\omega) & G^{+-}_{f_2\mu}(\omega)G^{+-}_{\nu h_2}(\Omega-\omega)\end{pmatrix},
\end{aligned}
\tag{2.34}
$$

where $f$ and $h$ are either $a$ or $b$. The parallel and perpendicular components correspond to diagonal and off-diagonal parts in the terms of the second order of $\gamma_{\pm1,2}$, respectively.

The abovementioned derivations of the current and the noise spectrum are simple extensions of a SQD, given in [29], to a DQD. We consider the effect of the Klein factor, which we had ignored while deriving the refermionized Hamiltonian. Without the Klein factor, the Hamiltonian is simply divided into unperturbed and perturbed parts by using the Majorana fermions. For a SQD connected with LL electrodes, there is no serious effect from neglecting the Klein factor. Contrary to it, if the Klein factor is taken into consideration for a DQD, the order of electron tunneling into quantum dots becomes important. By using the renormalization group method, it is shown that the current does not flow in an asymmetric parallel DQD; for an asymmetric tunnel coupling, the model flows to fixed points at which one of the tunnel amplitudes is zero [38]. This suggests that the Fermi statistics of electrons plays an important role through the Klein factor. In the bosonization and refermionization processes, we neglected the Klein factor, so the Fermi statistics of electrons does not hold. The influence of the absence of the Klein factor on our results is discussed in section 3.

In the following subsections, we derive Green's functions for the Majorana fermions by using the $S$-matrix expansion and the Dyson equations.

### 2.3. Green's functions for DQD

In order to numerically calculate the current and noise spectrum, it is necessary to determine Green's functions. We briefly explain the derivation of Green's functions by perturbation up to the second order of $\gamma_{\pm1,2}$.

First, in order to obtain the current (2.29), it is necessary to derive advanced Green's functions $D^{\mathrm{a}}_{fh}$. From the Dyson equations for each Green's function, $D^{\mathrm{a}}_{fh}$ are formulated in a 4 $\times$ 4 matrix form as

$$
\mathbf{A}^{\mathrm{a}}\mathbf{D}^{\mathrm{a}} = \mathbf{D}^{(0)\mathrm{a}},
\tag{2.35}
$$

where

$$\mathbf{A}^{\mathrm{a}} \equiv \begin{pmatrix} A^{\mathrm{a}}_{a_1a_1} & A^{\mathrm{a}}_{a_1b_1} & A^{\mathrm{a}}_{a_1a_2} & A^{\mathrm{a}}_{a_1b_2} \\ A^{\mathrm{a}}_{b_1a_1} & A^{\mathrm{a}}_{b_1b_1} & A^{\mathrm{a}}_{b_1a_2} & A^{\mathrm{a}}_{b_1b_2} \\ A^{\mathrm{a}}_{a_2a_1} & A^{\mathrm{a}}_{a_2b_1} & A^{\mathrm{a}}_{a_2a_2} & A^{\mathrm{a}}_{a_2b_2} \\ A^{\mathrm{a}}_{b_2a_1} & A^{\mathrm{a}}_{b_2b_1} & A^{\mathrm{a}}_{b_2a_2} & A^{\mathrm{a}}_{b_2b_2} \end{pmatrix},$$

$$\mathbf{D}^{\mathrm{a}} \equiv \begin{pmatrix} D^{\mathrm{a}}_{a_1a_1} & D^{\mathrm{a}}_{a_1b_1} & D^{\mathrm{a}}_{a_1a_2} & D^{\mathrm{a}}_{a_1b_2} \\ D^{\mathrm{a}}_{b_1a_1} & D^{\mathrm{a}}_{b_1b_1} & D^{\mathrm{a}}_{b_1a_2} & D^{\mathrm{a}}_{b_1b_2} \\ D^{\mathrm{a}}_{a_2a_1} & D^{\mathrm{a}}_{a_2b_1} & D^{\mathrm{a}}_{a_2a_2} & D^{\mathrm{a}}_{a_2b_2} \\ D^{\mathrm{a}}_{b_2a_1} & D^{\mathrm{a}}_{b_2b_1} & D^{\mathrm{a}}_{b_2a_2} & D^{\mathrm{a}}_{b_2b_2} \end{pmatrix}, \tag{2.36}$$

$$\mathbf{D}^{(0)\mathrm{a}} \equiv \begin{pmatrix} D^{(0)\mathrm{a}}_{a_1a_1} & D^{(0)\mathrm{a}}_{a_1b_1} & D^{(0)\mathrm{a}}_{a_1a_2} & D^{(0)\mathrm{a}}_{a_1b_2} \\ D^{(0)\mathrm{a}}_{b_1a_1} & D^{(0)\mathrm{a}}_{b_1b_1} & D^{(0)\mathrm{a}}_{b_1a_2} & D^{(0)\mathrm{a}}_{b_1b_2} \\ D^{(0)\mathrm{a}}_{a_2a_1} & D^{(0)\mathrm{a}}_{a_2b_1} & D^{(0)\mathrm{a}}_{a_2a_2} & D^{(0)\mathrm{a}}_{a_2b_2} \\ D^{(0)\mathrm{a}}_{b_2a_1} & D^{(0)\mathrm{a}}_{b_2b_1} & D^{(0)\mathrm{a}}_{b_2a_2} & D^{(0)\mathrm{a}}_{b_2b_2} \end{pmatrix}.$$

Here, the matrix elements of $\mathbf{A}^{\mathrm{a}}$ are

$$\begin{aligned} A^{\mathrm{a}}_{f_ia_j} &= -\gamma_{-j} \sum_{k=1,2} \gamma_{-k} D^{(0)\mathrm{a}}_{f_ia_k} G^{(0)\mathrm{a}}_{\eta\eta}, \\ A^{\mathrm{a}}_{f_ib_j} &= -\gamma_{+j} \sum_{k=1,2} \gamma_{+k} D^{(0)\mathrm{a}}_{f_ib_k} G^{(0)\mathrm{a}}_{\zeta\zeta}, \\ A^{\mathrm{a}}_{a_ia_i} &= 1 - \gamma_{-i} \sum_{k=1,2} \gamma_{-k} D^{(0)\mathrm{a}}_{a_ia_k} G^{(0)\mathrm{a}}_{\eta\eta}, \\ A^{\mathrm{a}}_{b_ib_i} &= 1 - \gamma_{+i} \sum_{k=1,2} \gamma_{+k} D^{(0)\mathrm{a}}_{b_ib_k} G^{(0)\mathrm{a}}_{\zeta\zeta}, \end{aligned} \tag{2.37}$$

where $f$ is either $a$ or $b$, and $i$ and $j$ are either 1 or 2. We can obtain the advanced Green's functions by solving equation (2.35). For the retarded Green's functions $D^{\mathrm{r}}_{fh}$, similar equations can be obtained by replacing the superscript a with r in equation (2.35).

Second, in order to obtain the noise spectrum, it is necessary to derive the greater Green's functions $D^{+-}_{fh}$. Using the Dyson equation and the analytic continuation rules, $D^{+-}_{fh}$ are formulated in the matrix form as

$$\mathbf{A}^{+-}\mathbf{D}^{+-} = \mathbf{C}^{+-}, \tag{2.38}$$

where

$$\mathbf{A}^{+-} \equiv \begin{pmatrix} A^{+-}_{a_1a_1} & A^{+-}_{a_1b_1} & A^{+-}_{a_1a_2} & A^{+-}_{a_1b_2} \\ A^{+-}_{b_1a_1} & A^{+-}_{b_1b_1} & A^{+-}_{b_1a_2} & A^{+-}_{b_1b_2} \\ A^{+-}_{a_2a_1} & A^{+-}_{a_2b_1} & A^{+-}_{a_2a_2} & A^{+-}_{a_2b_2} \\ A^{+-}_{b_2a_1} & A^{+-}_{b_2b_1} & A^{+-}_{b_2a_2} & A^{+-}_{b_2b_2} \end{pmatrix},$$

$$\mathbf{D}^{+-} \equiv \begin{pmatrix} D^{+-}_{a_1a_1} & D^{+-}_{a_1b_1} & D^{+-}_{a_1a_2} & D^{+-}_{a_1b_2} \\ D^{+-}_{b_1a_1} & D^{+-}_{b_1b_1} & D^{+-}_{b_1a_2} & D^{+-}_{b_1b_2} \\ D^{+-}_{a_2a_1} & D^{+-}_{a_2b_1} & D^{+-}_{a_2a_2} & D^{+-}_{a_2b_2} \\ D^{+-}_{b_2a_1} & D^{+-}_{b_2b_1} & D^{+-}_{b_2a_2} & D^{+-}_{b_2b_2} \end{pmatrix}, \tag{2.39}$$

$$\mathbf{C}^{+-} \equiv \begin{pmatrix} C^{+-}_{a_1a_1} & C^{+-}_{a_1b_1} & C^{+-}_{a_1a_2} & C^{+-}_{a_1b_2} \\ C^{+-}_{b_1a_1} & C^{+-}_{b_1b_1} & C^{+-}_{b_1a_2} & C^{+-}_{b_1b_2} \\ C^{+-}_{a_2a_1} & C^{+-}_{a_2b_1} & C^{+-}_{a_2a_2} & C^{+-}_{a_2b_2} \\ C^{+-}_{b_2a_1} & C^{+-}_{b_2b_1} & C^{+-}_{b_2a_2} & C^{+-}_{b_2b_2} \end{pmatrix}.$$

Here, the matrix elements of $\mathbf{A}^{+-}$ are

$$\begin{aligned} A^{+-}_{f_ia_j} &= -\gamma_{-j} \sum_{k=1,2} \gamma_{-k} D^{(0)\mathrm{r}}_{f_ia_k} G^{(0)\mathrm{r}}_{\eta\eta}, \\ A^{+-}_{f_ib_j} &= -\gamma_{+j} \sum_{k=1,2} \gamma_{+k} D^{(0)\mathrm{r}}_{f_ib_k} G^{(0)\mathrm{r}}_{\zeta\zeta}, \\ A^{+-}_{a_ia_i} &= 1 - \gamma_{-i} \sum_{k=1,2} \gamma_{-k} D^{(0)\mathrm{r}}_{a_ia_k} G^{(0)\mathrm{r}}_{\eta\eta}, \\ A^{+-}_{b_ib_i} &= 1 - \gamma_{+i} \sum_{k=1,2} \gamma_{+k} D^{(0)\mathrm{r}}_{b_ib_k} G^{(0)\mathrm{r}}_{\zeta\zeta}. \end{aligned} \tag{2.40}$$

The matrix elements of $\mathbf{C}^{+-}$ are

$$\begin{aligned} C^{+-}_{fh} = C^{(0)+-}_{fh} &+ \sum_{k,l=1,2} \gamma_{+k}\gamma_{+l} D^{(0)\mathrm{r}}_{fb_k} G^{(0)+-}_{\zeta\zeta} D^{\mathrm{a}}_{b_lh} \\ &+ \sum_{k,l=1,2} \gamma_{-k}\gamma_{-l} D^{(0)\mathrm{r}}_{fa_k} G^{(0)+-}_{\eta\eta} D^{\mathrm{a}}_{a_lh} \\ &+ \sum_{k,l=1,2} \gamma_{+k}\gamma_{-l} D^{(0)\mathrm{r}}_{fb_k} G^{(0)+-}_{\zeta\eta} D^{\mathrm{a}}_{a_lh} \\ &+ \sum_{k,l=1,2} \gamma_{-k}\gamma_{+l} D^{(0)\mathrm{r}}_{fa_k} G^{(0)+-}_{\eta\zeta} D^{\mathrm{a}}_{b_lh}, \end{aligned} \tag{2.41}$$

where $f$ and $h$ are either $a_{1,2}$ or $b_{1,2}$.

For the electrode Majorana Green's functions $G_{\mu\nu}$, we can derive the Dyson equation in a similar way. The advanced Green's functions $G^{\mathrm{a}}_{\mu\nu}$ are formulated in the matrix form as

$$\mathbf{M}^{\mathrm{a}}\boldsymbol{\Xi}^{\mathrm{a}} = \boldsymbol{\Xi}^{(0)\mathrm{a}}, \tag{2.42}$$

where

$$\mathbf{M}^{\mathrm{a}} \equiv \begin{pmatrix} M^{\mathrm{a}}_{a_1a_1} & M^{\mathrm{a}}_{a_1b_1} & 0 & 0 \\ M^{\mathrm{a}}_{b_1a_1} & M^{\mathrm{a}}_{b_1b_1} & 0 & 0 \\ 0 & 0 & M^{\mathrm{a}}_{a_2a_2} & M^{\mathrm{a}}_{a_2b_2} \\ 0 & 0 & M^{\mathrm{a}}_{b_2a_2} & M^{\mathrm{a}}_{b_2b_2} \end{pmatrix},$$

$$\boldsymbol{\Xi}^{\mathrm{a}} \equiv \begin{pmatrix} G^{\mathrm{a}}_{\eta\eta} \\ G^{\mathrm{a}}_{\zeta\eta} \\ G^{\mathrm{a}}_{\eta\zeta} \\ G^{\mathrm{a}}_{\zeta\zeta} \end{pmatrix}, \qquad \boldsymbol{\Xi}^{(0)\mathrm{a}} \equiv \begin{pmatrix} G^{(0)\mathrm{a}}_{\eta\eta} \\ G^{(0)\mathrm{a}}_{\zeta\eta} \\ G^{(0)\mathrm{a}}_{\eta\zeta} \\ G^{(0)\mathrm{a}}_{\zeta\zeta} \end{pmatrix}. \tag{2.43}$$

Here, the matrix elements of $\mathbf{M}^{\mathrm{a}}$ are

$$\begin{aligned} M^{\mathrm{a}}_{a_ib_i} &= -\sum_{k,l=1,2} \gamma_{-k}\gamma_{+l} D^{(0)\mathrm{a}}_{a_kb_l} G^{(0)\mathrm{a}}_{\eta\eta}, \\ M^{\mathrm{a}}_{b_ia_i} &= -\sum_{k,l=1,2} \gamma_{+k}\gamma_{-l} D^{(0)\mathrm{a}}_{b_ka_l} G^{(0)\mathrm{a}}_{\zeta\zeta}, \\ M^{\mathrm{a}}_{a_ia_i} &= 1 - \sum_{k,l=1,2} \gamma_{-k}\gamma_{-l} D^{(0)\mathrm{a}}_{a_ka_l} G^{(0)\mathrm{a}}_{\eta\eta}, \\ M^{\mathrm{a}}_{b_ib_i} &= 1 - \sum_{k,l=1,2} \gamma_{+k}\gamma_{+l} D^{(0)\mathrm{a}}_{b_kb_l} G^{(0)\mathrm{a}}_{\zeta\zeta}. \end{aligned} \tag{2.44}$$

In contrast, for the greater Green's functions, $G^{+-}_{\mu\nu}$ are formulated as

$$\mathbf{M}^{+-}\boldsymbol{\Xi}^{+-} = \mathbf{B}^{+-}, \tag{2.45}$$

where

$$\mathbf{M}^{+-} \equiv \begin{pmatrix} M^{+-}_{a_1a_1} & M^{+-}_{a_1b_1} & 0 & 0 \\ M^{+-}_{b_1a_1} & M^{+-}_{b_1b_1} & 0 & 0 \\ 0 & 0 & M^{+-}_{a_2a_2} & M^{+-}_{a_2b_2} \\ 0 & 0 & M^{+-}_{b_2a_2} & M^{+-}_{b_2b_2} \end{pmatrix},$$
$$\boldsymbol{\Xi}^{+-} \equiv \begin{pmatrix} G^{+-}_{\eta\eta} \\ G^{+-}_{\zeta\eta} \\ G^{+-}_{\eta\zeta} \\ G^{+-}_{\zeta\zeta} \end{pmatrix}, \qquad \mathbf{B}^{+-} \equiv \begin{pmatrix} B^{+-}_{\eta\eta} \\ B^{+-}_{\zeta\eta} \\ B^{+-}_{\eta\zeta} \\ B^{+-}_{\zeta\zeta} \end{pmatrix}. \tag{2.46}$$

Here, the matrix elements of $\mathbf{M}^{+-}$ are

$$\begin{aligned} M^{+-}_{a_ib_i} &= -\sum_{k,l=1,2} \gamma_{-k}\gamma_{+l} D^{(0)\mathrm{r}}_{a_kb_l} G^{(0)\mathrm{r}}_{\eta\eta}, \\ M^{+-}_{b_ia_i} &= -\sum_{k,l=1,2} \gamma_{+k}\gamma_{-l} D^{(0)\mathrm{r}}_{b_ka_l} G^{(0)\mathrm{r}}_{\zeta\zeta}, \\ M^{+-}_{a_ia_i} &= 1-\sum_{k,l=1,2} \gamma_{-k}\gamma_{-l} D^{(0)\mathrm{r}}_{a_ka_l} G^{(0)\mathrm{r}}_{\eta\eta}, \\ M^{+-}_{b_ib_i} &= 1-\sum_{k,l=1,2} \gamma_{+k}\gamma_{+l} D^{(0)\mathrm{r}}_{b_kb_l} G^{(0)\mathrm{r}}_{\zeta\zeta}, \end{aligned} \tag{2.47}$$

and the $B^{+-}_{\mu\nu}$ are

$$\begin{aligned} B^{+-}_{\mu\nu} &= G^{(0)+-}_{\mu\nu} + \sum_{k,l=1,2} \gamma_{+k}\gamma_{+l} G^{(0)+-}_{\mu\zeta} D^{(0)\mathrm{a}}_{b_kb_l} G^{\mathrm{a}}_{\zeta\nu} \\ &+ \sum_{k,l=1,2} \gamma_{-k}\gamma_{-l} G^{(0)+-}_{\mu\eta} D^{(0)\mathrm{a}}_{a_ka_l} G^{\mathrm{a}}_{\eta\nu} \\ &+ \sum_{k,l=1,2} \gamma_{+k}\gamma_{-l} G^{(0)+-}_{\mu\zeta} D^{(0)\mathrm{a}}_{b_ka_l} G^{\mathrm{a}}_{\eta\nu} \\ &+ \sum_{k,l=1,2} \gamma_{-k}\gamma_{+l} G^{(0)+-}_{\mu\eta} D^{(0)\mathrm{a}}_{a_kb_l} G^{\mathrm{a}}_{\zeta\nu}, \end{aligned} \tag{2.48}$$

where $\mu$ and $\nu$ are either $\zeta$ or $\eta$.

$G^{\pm}_{f\mu;\nu h}$ denotes the Green's functions between different subsystems of the Majorana fermions ($a$–$b$ and $\zeta$–$\eta$ subsystems). In order to express them in terms of the same subsystem, the $S$-matrix expansion is utilized. We obtain the relations

$$\begin{aligned} G^{+-}_{f_i\eta} &= -\tfrac{1}{2}F\mathrm{i}\sum_{k=1,2}\gamma_{+k}D^{\mathrm{r}}_{f_ib_k} - \mathrm{i}\sum_{k=1,2}\gamma_{-k}D^{+-}_{f_ia_k}G^{(0)\mathrm{a}}_{\eta\eta} \\ &\quad - \mathrm{i}\sum_{k=1,2}\gamma_{-k}D^{\mathrm{r}}_{f_ia_k}G^{(0)+-}_{\eta\eta}, \\ G^{+-}_{f_i\zeta} &= \tfrac{1}{2}F\mathrm{i}\sum_{k=1,2}\gamma_{-k}D^{\mathrm{r}}_{f_ia_k} - \mathrm{i}\sum_{k=1,2}\gamma_{+k}D^{+-}_{f_ib_k}G^{(0)\mathrm{a}}_{\zeta\zeta} \\ &\quad - \mathrm{i}\sum_{k=1,2}\gamma_{+k}D^{\mathrm{r}}_{f_ib_k}G^{(0)+-}_{\zeta\zeta}, \\ G^{+-}_{\eta f_i} &= -\tfrac{1}{2}F\mathrm{i}\sum_{k=1,2}\gamma_{+k}D^{\mathrm{a}}_{b_kf_i} + \mathrm{i}\sum_{k=1,2}\gamma_{-k}D^{\mathrm{a}}_{a_kf_i}G^{(0)+-}_{\eta\eta} \\ &\quad + \mathrm{i}\sum_{k=1,2}\gamma_{-k}D^{+-}_{a_kf_i}G^{(0)\mathrm{r}}_{\eta\eta}, \\ G^{+-}_{\zeta f_i} &= \tfrac{1}{2}F\mathrm{i}\sum_{k=1,2}\gamma_{-k}D^{\mathrm{a}}_{a_kf_i} + \mathrm{i}\sum_{k=1,2}\gamma_{+k}D^{\mathrm{a}}_{b_kf_i}G^{(0)+-}_{\zeta\zeta} \\ &\quad + \mathrm{i}\sum_{k=1,2}\gamma_{+k}D^{+-}_{b_kf_i}G^{(0)\mathrm{r}}_{\zeta\zeta}, \end{aligned} \tag{2.49}$$

where $f$ is either $a$ or $b$. Using these relations, we can obtain $G^{\pm}_{b\eta;\eta b}$.

Thus, we derived the Green's functions of the Majorana fermions. Substituting them into equations (2.29) and (2.31), we can calculate the current and the noise spectrum, respectively.

## 3. Numerical results

In section 2.3, we have derived the Green's functions by the perturbation expansion. Using those Green's functions, the current is given in the Landauer formula [39] as

$$\begin{aligned} I &= \frac{e}{\hbar}\frac{\Gamma}{2\pi}\int \mathrm{d}\omega\, T(\omega)[n_{\mathrm{F}}(\omega - eV) - n_{\mathrm{F}}(\omega)] \\ &\equiv \frac{e}{h}\int \mathrm{d}\omega\, T(\omega)[n_{\mathrm{F}}(\omega - eV) - n_{\mathrm{F}}(\omega)], \end{aligned} \tag{3.1}$$

where $T(\omega)$ is the transmission probability, and all energy variables are scaled by $\Gamma$. On the other hand, the noise spectrum is generally calculated by using the complete set of Green's functions. However, for the symmetric coupling case, $P_{\perp}(\Omega) = 0$, so that the noise spectrum at $\Omega = 0$ is described in a simple form as

$$P(0) = \frac{2e^2}{h}\int \mathrm{d}\omega\, T(\omega)(1 - T(\omega))[n_{\mathrm{F}}(\omega - eV) - n_{\mathrm{F}}(\omega)]. \tag{3.2}$$

We note that this formula at zero temperature has a similar form to the formula for noninteracting electrons [9, 40]. We remark that the shot noise for the asymmetric coupling case cannot be described in a simple form (3.2); it must be calculated by using the complete set of Green's functions. In the following subsections, we obtain the explicit expression of the transmission probability for a SQD and T-shaped and parallel DQD systems, and discuss the dependence of the Fano factor on the bias voltage, the energy levels of dots, the interdot coupling, and the asymmetry parameter. In the numerical calculations, we restrict $\Delta_{1,2}$ and $W$ in the range $\Delta_{1,2} \geqslant 0$ and $W \geqslant 0$, unless otherwise stated.

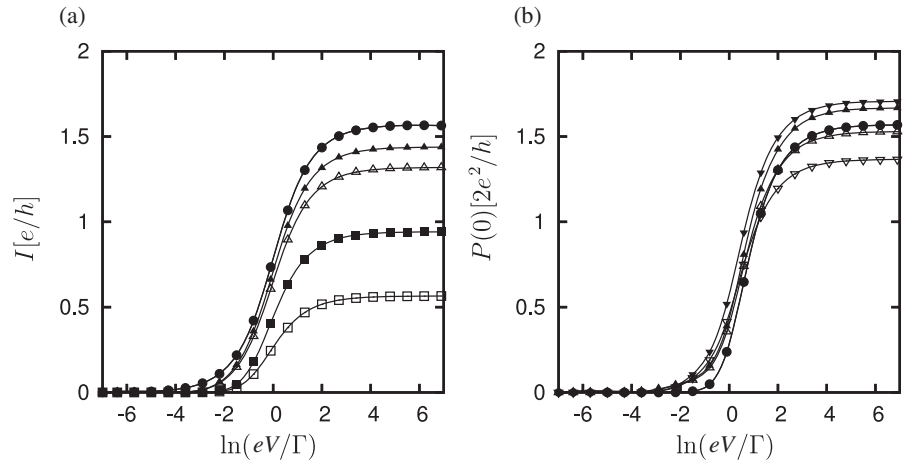


**Figure 3.** Dependence of (a) current and (b) shot noise in the zero-frequency limit in SQD on bias voltage. $\Delta_1 = 0$. Curves denoted by ○, △, ▽, and □ correspond to cases $\alpha = 0.5$, 0.3, 0.2, and 0.1, respectively, which are obtained by using the exact transmission probability (3.3). Curves denoted by ●, ▲, ▼, and ■ correspond to cases $\alpha = 0.5$, 0.3, 0.2, and 0.1, respectively, which are obtained by using the approximate transmission probability (3.5) and the complete set of Green's functions.

### *3.1. SQD*

We first consider the case $\gamma_{\pm 2} = 0$ and $W = 0$. In this case, our DQD system describes a SQD system. The asymmetry parameter $\alpha$ is defined by $\alpha = \frac{\gamma_{\mathrm{I,L}}^2}{\gamma_{\mathrm{I,L}}^2+\gamma_{\mathrm{I,R}}^2}$, and all energy variables are scaled by $\Gamma = \gamma_{\mathrm{I,L}}^2 + \gamma_{\mathrm{I,R}}^2$ ($\equiv\gamma_0^2$). For the transmission probability and shot noise, the results do not change under the replacement $\alpha \leftrightarrow (1-\alpha)$. Thus, we restrict $\alpha$ in the range $0 \leqslant \alpha \leqslant 0.5$. In order to verify the validity of the perturbation calculation, we compare the currents and the Fano factors obtained by two different methods—using the exact transmission probability and using perturbation calculations.

The exact transmission probability of this quantum dot system is obtained by using the equation of motion method [22]:

$$T_{\mathrm{e}}(\omega) = \frac{4\gamma^2 E^2}{(E^2+\beta_+^2)(E^2+\beta_-^2)+2\gamma^2(E^2+\beta_+\beta_-)+\gamma^4}, \tag{3.3}$$

where

$$E = (\omega^2 - \Delta_1^2), \qquad \beta_\pm = [(1-2\alpha)\Delta_1 \pm \omega]/2, \qquad \gamma = \omega\sqrt{\alpha(1-\alpha)}. \tag{3.4}$$

On the other hand, using Green's functions obtained by perturbation expansion, we can derive the approximate transmission probability as

$$T(\omega) = \frac{2\sqrt{\alpha(1-\alpha)}\omega^2}{[E+\frac{1}{4}+\alpha(1-\alpha)]^2+\Delta_1^2-\alpha(1-\alpha)}. \tag{3.5}$$

We can verify that $T(\omega)$ agrees with $T_{\mathrm{e}}(\omega)$ only for $\alpha = 0.5$. The current is given by the Landauer formula (3.1). The dependence of the current on bias voltage for $\Delta_1 = 0$ is shown in figure 3(a). Although currents obtained by using the transmission probabilities (3.3) and (3.5) agree completely when $\alpha = 0.5$, the difference between the currents obtained by two different methods is large for small $\alpha$.

Second, we discuss the shot noise. For $\Delta_1 = 0$, the shot noise in the zero-frequency limit is calculated using the exact transmission probability $T_{\mathrm{e}}$ as [29]

$$P_{\mathrm{e}}(0) = \frac{2e^2}{h}\int \mathrm{d}\omega\, T_{\mathrm{e}}(\omega)(1-T_{\mathrm{e}}(\omega))[n_{\mathrm{F}}(\omega-eV)-n_{\mathrm{F}}(\omega)]. \tag{3.6}$$

Equation (3.6) is of the same form as that of the noninteracting case. For $g = 1/2$, the original Hamiltonian (2.1) is mapped to the refermionized Hamiltonian (2.16). At the Toulouse point, it describes free fermions which scatter at $x = 0$. Thus, we can guess that the resulting formula for shot noise is same as that of the noninteracting system. We compare the shot noise obtained by using equation (3.6) and the perturbation calculation. At zero temperature, the shot noise obtained by the two different methods is shown in figure 3(b). Similar to the results for current, the difference between the shot noise obtained by two methods is large for small $\alpha$.

At zero temperature, the shot noise Fano factor $F(V) = P(0)/2eI$ is used to characterize the deviation from the Poisson value $2eI$. The dependence of the Fano factor on bias voltage is shown in figure 4. The data were calculated by using two different methods for fixed $\Delta_1$ or $\alpha$. For $\Delta_1 = 0$, there is no difference between the values calculated by using the two methods (figure 4(a-i)). However, in the case of large $\Delta_1$, a difference is observed for small $\alpha$ only at a low bias voltage (figure 4(a-ii)). For $\alpha = 0.5$ but $\Delta_1 \neq 0$, the shot noise is given by equation (3.6). The Fano factor for different $\Delta_1$ is shown in figure 4(b-i). The Fano factor shows a monotonic behavior for $\Delta_1 = 0$, but it shows a nonmonotonic behavior with a local minimum for $\Delta_1 \neq 0$. We can also verify that the difference between the values is large for small $\alpha$ and large $\Delta_1$, and the difference is observed only at a low bias voltage (compare figure 4(b-i) with (b-ii)).

The properties of the Fano factor in a SQD are such that the noise is sub-Poissonian, and only under resonance for $\alpha = 0.5$ and $\Delta_1 = 0$ does the Fano factor show a monotonic behavior with bias voltage. For other values of $\alpha$ and $\Delta_1$,

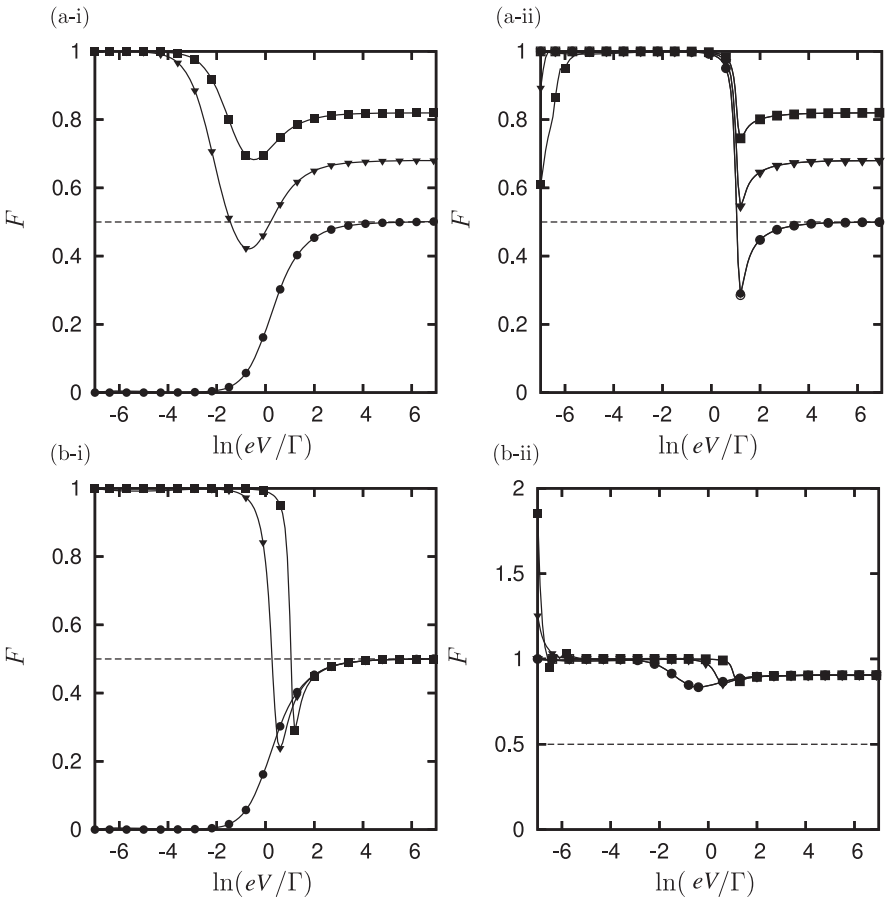


**Figure 4.** Dependence of Fano factor in SQD on bias voltage. (a) $\Delta_1$ is fixed case: (a-i) $\Delta_1 = 0$ and (a-ii) $\Delta_1 = 3$. Curves denoted by ○, ▽, and □ correspond to cases $\alpha = 0.5$, 0.2, and 0.1, respectively, which are obtained by using the exact transmission probability. Curves denoted by ●, ▼, and ■ correspond to cases $\alpha = 0.5$, 0.2, and 0.1, respectively, which are obtained by using the approximate transmission probability and the complete set of Green's functions. (b) $\alpha$ is fixed case: (b-i) $\alpha = 0.5$ and (b-ii) $\alpha = 0.05$. Curves denoted by ○, ▽, and □ correspond to cases $\Delta_1 = 0.0$, 1.5, and 3.0, respectively, which are obtained by using the exact transmission probability. Curves denoted by ●, ▼, and ■ correspond to cases $\Delta_1 = 0.0$, 1.5, and 3.0, respectively, which are obtained by using the approximate transmission probability and complete set of Green's functions.

the Fano factor shows a nonmonotonic behavior, and a local minimum occurs in the intermediate voltage range. From the definition of the Fano factor, we find that the local minimum at $V = V^*$ satisfies the relation $F(V^*) = (1 - T(eV^*))$. The small bias limit of the Fano factor is $F(0) = 0$ and 1 for $\alpha = 0.5$ and $0 \leqslant \alpha < 0.5$, respectively. In contrast, the large bias limit does not depend on $\Delta_1$, but only on $\alpha$, $F(\infty) = 2\alpha^2 - 2\alpha + 1$ [29]. Let us compare these results with other systems. The Fano factor for double barrier resonant tunneling in a noninteracting Fermi liquid was studied in [41]. In this case, the shot noise is sub-Poissonian, and the Fano factor shows a monotonic behavior with bias voltage. The limiting values are $F(0) = (2\alpha - 1)^2$ and $F(\infty) = 2\alpha^2 - 2\alpha + 1$. Thus, the behavior of the Fano factor in the large bias limit $F(\infty)$ is same as that of the noninteracting Fermi liquid. The nonmonotonic behavior of the Fano factor in the LL with two barriers was studied in [42]. In that study, for large asymmetric barriers, a series of dips (local minima) are observed, and the Fano factor saturates to a constant value with increasing bias voltage. This results from the interplay between Coulomb blockade features and non-Fermi liquid correlations. On the other hand, the intradot Coulomb interaction is not taken into consideration in our model. The local minima occurs when the abovementioned relation between the transmission probability and the Fano factor is satisfied self-consistently. This suggests that the occurrence of a dip in this model is closely related with the profile of the transmission probability.

Thus, for the asymmetric coupling case, the current and the shot noise obtained by using the second order perturbation expansion are larger than the exact solution. However, the Fano factor agrees well with the exact result, except at a low bias voltage. The difference at a low bias voltage is large for cases of small $\alpha$ and large $\Delta_1$. We guess that the reason for the agreement of the Fano factor is the cancelation by the division between the shot noise and the current. Taking these preliminary studies of a SQD into consideration, we calculate the Fano factor for symmetric and asymmetric coupling cases of T-shaped and parallel DQDs by using a complete set of Green's functions. For the symmetric coupling case, the dependence of the Fano factor on the energy levels of the dots and the interdot coupling is studied on the basis of the profile of the transmission probability. Furthermore, for a parallel DQD,

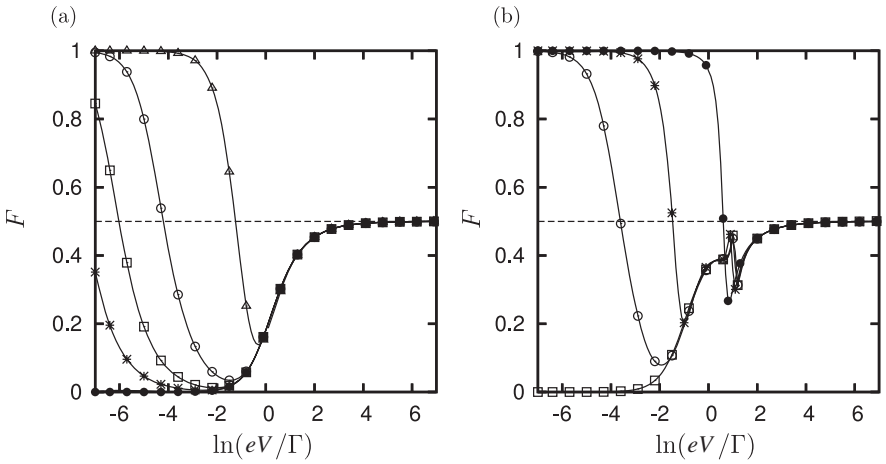


**Figure 5.** Dependence of the Fano factor in T-shaped DQD on bias voltage for different energy levels of dots and interdot coupling. $\alpha = 0.5$. (a) $\Delta_1 = \Delta_2 = 0$. Curves denoted by ●, ∗, □, ○, and △ correspond to cases $W = 0.0$, 0.02, 0.04, 0.1, and 0.5, respectively. (b) $\Delta_1 = 2.0$ and $\Delta_2 = 1.0$. Curves denoted by ●, ∗, □, and ○ correspond to cases $W = 0.0$, 1.1, $\sqrt{2.0}$, and 1.5, respectively.

two types of asymmetry are considered, and the limitation of the perturbation calculation is discussed.

### *3.2. T-shaped DQD*

The transmission probability for the T-shaped DQD obtained by the perturbation expansion is

$$T(\omega) = \frac{2\sqrt{\alpha(1-\alpha)}F_{\mathrm{T1}}^2}{[D - (\alpha - \frac{1}{2})^2 F_{\mathrm{T2}}]^2 + F_{\mathrm{T1}}^2}, \tag{3.7}$$

where

$$F_{\mathrm{T1}} = \omega(\omega^2 - \Delta_2^2 - W^2), \qquad F_{\mathrm{T2}} = (\omega^2 - \Delta_2^2). \tag{3.8}$$

The asymmetry parameter $\alpha$ is defined by $\alpha = \frac{\gamma_{\mathrm{l,L}}^2}{\gamma_{\mathrm{l,L}}^2 + \gamma_{\mathrm{l,R}}^2}$, and all energy variables are scaled by $\Gamma = (\gamma_{\mathrm{l,L}}^2 + \gamma_{\mathrm{l,R}}^2)$.

For the symmetric coupling case, the shot noise is described by a simple form (3.2). The behavior of the Fano factor can be easily understood from the profile of the transmission probability. Therefore, we first examine the transmission probability for the symmetric coupling case. Substituting $\alpha = 0.5$, the transmission probability $T(\omega)$ becomes

$$T(\omega) = \frac{F_{\mathrm{T1}}(\omega)^2}{D(\omega)^2 + F_{\mathrm{T1}}(\omega)^2}. \tag{3.9}$$

This transmission probability has three local minima at $\omega = 0, \pm\sqrt{\Delta_2^2 + W^2}$ and four local maxima at $\omega = \pm\frac{1}{2}[(\Delta_1 + \Delta_2) \pm \sqrt{(\Delta_1 - \Delta_2)^2 + 4W^2}]$. The degenerate local extrema result in different profiles. For $\Delta_1 = \Delta_2 = W = 0$, $T(\omega)$ has one local maximum at $\omega = 0$. However, for $W \neq 0$, $T(\omega)$ has two local maxima at $\omega = \pm W$ and one local minimum at $\omega = 0$. For $W = 0$, $\Delta_1 \neq 0$, and $\Delta_2 = 0$, $T(\omega)$ has one local minimum at $\omega = 0$ and two local maxima at $\omega = \pm\Delta_1$. For $W \neq 0$, $T(\omega)$ has three local minima at $\omega = 0, \pm W$ and four local maxima at $\omega = \pm\frac{1}{2}[\Delta_1 \pm \sqrt{\Delta_1^2 + 4W^2}]$. The role of the energy levels of dots 1 and 2 is different. Let us exchange $\Delta_1$ and $\Delta_2$ such that $\Delta_1 = 0$ and $\Delta_2 \neq 0$. For $W = 0$, $T(\omega)$ has one local maximum at $\omega = 0$. For $W \neq 0$, $T(\omega)$ has three local minima at $\omega = 0, \pm\sqrt{\Delta_2^2 + W^2}$ and four local maxima at $\omega = \pm\frac{1}{2}[\Delta_2 \pm \sqrt{\Delta_2^2 + 4W^2}]$. For general values of $\Delta_{1,2}$ and $W$ ($\neq 0$), we find that when $W = \sqrt{\Delta_1\Delta_2}$ ($\equiv W^*$), the two local maxima approach $\omega = 0$. In this case, a local maximum around $\omega = 0$ has a sharp dip satisfying $T(0) = 0$. Thus, the interdot coupling causes four local maxima, except for the case $W = W^*$, in which three local maxima occur. At these local minima and maxima, $T(\omega)$ is 0 and 1. On the basis of these properties of the transmission probability, we discuss the Fano factor.

The dependence of the Fano factor on the bias voltage is shown in figure 5. First, let us consider the case $\Delta_1 = \Delta_2 = 0$. For $W = 0$, the Fano factor is strongly suppressed to 0 at a small voltage; however, it increases monotonically and saturates to 0.5 at a large voltage (figure 5(a)). For $W \neq 0$, the Fano factor increases at a small voltage. Because $T(0) = 0$ and two local maxima occur for $W > 0$, the Fano factor converges to 1 in the limit $V \to 0$. We find that the Fano factor has one local minimum for $W > 0$. We can show that the local minimal voltage $V^*$ satisfies $F(V^*) = (1 - T(eV^*))$. For general values of $\Delta_{1,2}$ ($\neq 0$), the dependence of the Fano factor on the bias voltage becomes more complex. In the case of $W = 0$, there is one solution for $F(V^*) = (1 - T(eV^*))$, so that one local minimum occurs in the Fano factor. On the other hand, for $W \neq 0$, $W^*$, two local minima and one local maximum occur in the Fano factor at intermediate voltage. In this case, there are four local maxima in $T(\omega)$. This results in three solutions for $F(V^*) = (1 - T(eV^*))$ in the range $V^* > 0$. Then, two local minima and one maximum occur in the Fano factor (figure 5(b)). However, for $W = W^*$, three local maxima occur in $T(\omega)$. One of them is located around $\omega = 0$, so that the Fano factor is strongly suppressed to 0 at a small voltage (curves denoted by □ in figure 5(b)). Thus, the nonmonotonic behavior of the Fano factor results from the complex structure of the transmission probability. The interdot

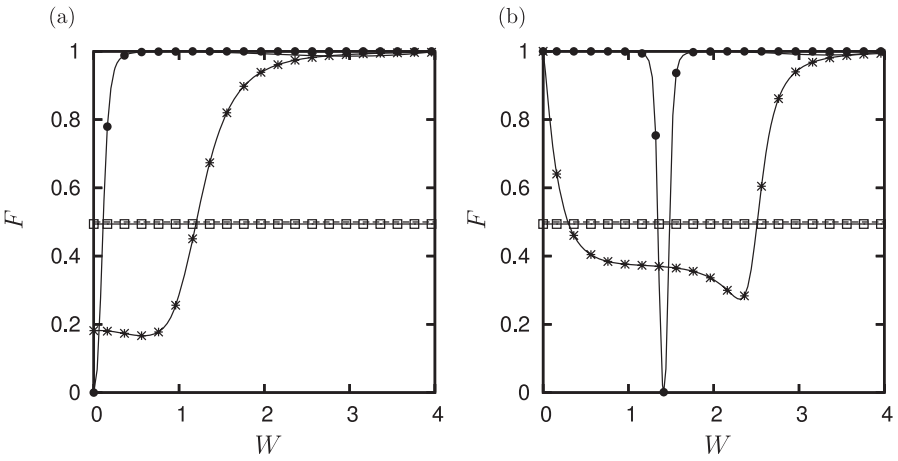


**Figure 6.** Dependence of Fano factor in T-shaped DQD on interdot coupling for different energy levels of dots and bias voltage. $\alpha = 0.5$. (a) $\Delta_1 = \Delta_2 = 0$ and (b) $\Delta_1 = 2.0$ and $\Delta_2 = 1.0$. Curves denoted by ●, ∗, and □ correspond to cases $\ln(eV/\Gamma) = -4.0$, 0.0, and 4.0, respectively.

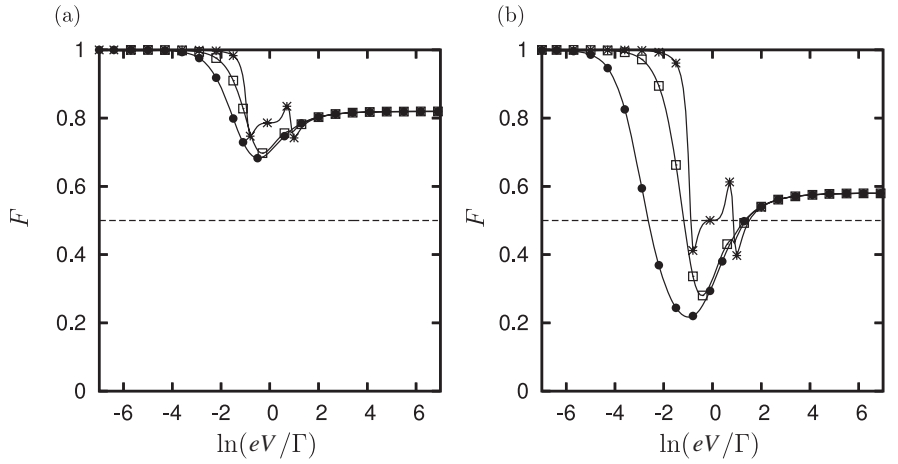


**Figure 7.** Dependence of Fano factor in T-shaped DQD on bias voltage for different energy levels of dots, interdot coupling, and asymmetry parameter. (a) $\alpha = 0.1$ and (b) $\alpha = 0.3$. Curves denoted by ●, ∗, and □ correspond to cases $(\Delta_1, \Delta_2, W) = (0, 0, 0)$, (2, 0, 1), and (0, 2, 1), respectively.

coupling causes the mixing of the bare energy levels of the dots, leading to the complex dependence of the transmission probability on these parameters.

The dependence of the Fano factor on interdot coupling is shown in figure 6. We explain three cases of different bias voltages. Let us consider the case of a small bias voltage (curves denoted by ●). For the case $\Delta_1 = \Delta_2 = 0$, $T(0) \to 1$ in the limit $W \to 0$, so that the Fano factor is 0. Increasing $W$, $T(0) = 0$, so that the Fano factor increases and saturates to 1 (figure 6(a)). For general values of $\Delta_{1,2}$ ($\neq 0$), $T(0) = 0$, so that the Fano factor is 1 in the limit $W \to 0$. Increasing $W$, four local maxima occur in $T(\omega)$. These are located away from $\omega = 0$, so that $T(\omega)$ around $\omega = 0$ is very small, and the Fano factor is 1. However, for $W = W^*$, one local maximum occurs around $\omega = 0$. Although this peak has a sharp dip satisfying $T(0) = 0$, $T(\omega)$ has a large value around $\omega = 0$, so that the Fano factor is strongly suppressed (figure 6(b)). When the bias voltage is in the intermediate range (curves denoted by ∗), the Fano factor changes nonmonotonically with $W$. The Fano factor in the limit $W \to 0$ varies depending on $\Delta_{1,2}$. Increasing $W$, four local maxima occur in $T(\omega)$, resulting in the nonmonotonic behavior of the Fano factor. For considerably large $W$, the maxima are located at $|\omega| \gg eV$ and $T(\omega) \sim 0$ in the range $|\omega| < eV$, so that the Fano factor saturates to 1 for any value of $\Delta_{1,2}$. When the bias voltage is large (curves denoted by □), the Fano factor is about 0.5 for any value of $\Delta_{1,2}$ and $W$.

Second, we consider the asymmetric coupling case, in which $\alpha \neq 0.5$. The dependence of the Fano factor on bias voltage is nonmonotonic, as shown in figure 7. The limiting values of the Fano factors are $F(0) = 1$ and $F(\infty) = 2\alpha^2 - 2\alpha + 1$, which are the same as those in case of a SQD. The only difference is that three local minima can occur in the intermediate voltage range.

### *3.3. Parallel DQD*

For the parallel DQD, the asymmetric parameters are defined by $\alpha_1 = \gamma_{1,\mathrm{L}}^2/(\gamma_{1,\mathrm{L}}^2 + \gamma_{1,\mathrm{R}}^2)$ and $\alpha_2 = \gamma_{2,\mathrm{L}}^2/(\gamma_{2,\mathrm{L}}^2 + \gamma_{2,\mathrm{R}}^2)$. We

assume $(\gamma_{1,\mathrm{L}}^2 + \gamma_{1,\mathrm{R}}^2) = (\gamma_{2,\mathrm{L}}^2 + \gamma_{2,\mathrm{R}}^2) \equiv \gamma_0^2$, and all energy variables are scaled by $\Gamma = \gamma_0^2$. We consider two types of asymmetric coupling: (i) $\alpha_1 = \alpha_2$ and (ii) $\alpha_1 = 1 - \alpha_2$. We note that for type (ii), in the limits $\alpha_1 \to 0$ and $\alpha_2 \to 1$, the parallel DQD is equivalent to a serial DQD with symmetric coupling.

First, we consider type (i), i.e., $\alpha_1 = \alpha_2 = \alpha$. The transmission probability obtained by the perturbation expansion is

$$T(\omega) = \frac{2\sqrt{\alpha(1-\alpha)}F_{\mathrm{s1}}^2 D^2}{[D^2 + (\alpha - \frac{1}{2})^2(F_{\mathrm{s2}}^2 - F_{\mathrm{s1}}^2)]^2 + D^2 F_{\mathrm{s1}}^2}, \tag{3.10}$$

where

$$\begin{aligned} F_{\mathrm{s1}} &= \omega[2\omega^2 - \Delta_1^2 - \Delta_2^2 - 2W^2 + 2W(\Delta_1 + \Delta_2)], \\ F_{\mathrm{s2}} &= (\Delta_1 + \Delta_2)(\omega^2 - \Delta_1\Delta_2 + W^2) \\ &\quad + 2W(\omega^2 + \Delta_1\Delta_2 - W^2). \end{aligned} \tag{3.11}$$

Our parallel DQD is equivalent to a SQD with two states. The exact transmission probability $T_{\mathrm{e}}(\omega)$ for a SQD with two states is obtained by using the equation of motion method in [29]. It is of the same form as equation (3.3), but the parameters are replaced by

$$\begin{aligned} E &= [(\omega - \Delta_1)(\omega - \Delta_2) - W^2][(\omega + \Delta_1)(\omega + \Delta_2) - W^2], \\ \gamma &= \omega\sqrt{\alpha(1-\alpha)}[-2\omega^2 + \Delta_1^2 + \Delta_2^2 \\ &\quad + 2W^2 - 2W(\Delta_1 + \Delta_2)], \\ \beta_\pm &= (\tfrac{1}{2} - \alpha)[(\Delta_1 + \Delta_2)(-\omega^2 + \Delta_1\Delta_2 - W^2) - 2W\omega^2] \\ &\quad \pm \frac{\gamma}{2\sqrt{\alpha(1-\alpha)}}. \end{aligned} \tag{3.12}$$

For the symmetric coupling case, $\alpha = 0.5$, $T_{\mathrm{e}}(\omega)$ agrees with $T(\omega)$, and $T(\omega)$ becomes

$$T(\omega) = \frac{F_{\mathrm{s1}}(\omega)^2}{D(\omega)^2 + F_{\mathrm{s1}}(\omega)^2}. \tag{3.13}$$

It is noted that the properties of the transmission probability and the shot noise do not change under the exchange of $\Delta_1$ and $\Delta_2$ due to the symmetry of the system. This transmission probability has three local minima at $\omega = 0, \pm\sqrt{\frac{1}{2}[(\Delta_1 - W)^2 + (\Delta_2 - W)^2]}$ and four local maxima at $\omega = \pm\frac{1}{2}[(\Delta_1 + \Delta_2) \pm \sqrt{(\Delta_1 - \Delta_2)^2 + 4W^2}]$. Consider the case of $\Delta_1 = \Delta_2 = 0$. For $W = 0$, $T(\omega)$ has one local maximum at $\omega = 0$. However, for $W \neq 0$, $T(\omega)$ has two local maxima at $\omega = \pm W$ and one local minimum at $\omega = 0$. Next, consider the case $\Delta_1 \neq 0$ and $\Delta_2 = 0$. For $W = 0$, $T(\omega)$ has two local minima at $\omega = \pm\Delta_1/\sqrt{2}$ and three local maxima at $\omega = 0, \pm\Delta_1$. For $W \neq 0$, $T(\omega)$ has three local minima at $\omega = 0, \pm\sqrt{\frac{1}{2}[(\Delta_1 - W)^2 + W^2]}$ and four local maxima at $\omega = \pm\frac{1}{2}[\Delta_1 \pm \sqrt{\Delta_1^2 + 4W^2}]$. For general values of $\Delta_{1,2}$ and $W$ ($\neq 0$), a pair of local minima and local maxima occur at the same positions when $\Delta_1 = \Delta_2 = \Delta$. As a result, $T(\omega)$ has one local minimum at $\omega = 0$ and two local maxima at $\omega = \pm(\Delta + W)$. On the other hand, for $\Delta_1 \neq \Delta_2$ and $W = \sqrt{\Delta_1\Delta_2}$ ($\equiv W^*$), two local maxima approach $\omega = 0$, forming a local maxima at $\omega = 0$ with a sharp dip satisfying $T(0) = 0$. We discuss the Fano factor on the basis of these properties of the transmission probability.

The dependence of the Fano factor on the bias voltage is shown in figure 8. The properties of the Fano factor are qualitatively the same as those of the case of the T-shaped DQD (figure 5). The only difference is that for the case $\Delta_1 = \Delta_2$ ($\neq 0$), the Fano factor is 1 for any value of $W$ at small bias voltage (figure 8(b)). In addition, only one local minimum occurs in the Fano factor. These are caused by the fact that $T(0) = 0$ for any value of $W$. Two local maxima occur in $T(\omega)$, and there is one solution for $F(V^*) = (1 - T(eV^*))$ in the range $V^* > 0$. This results in only one local minimum in the Fano factor.

The dependence of the Fano factor on the interdot coupling is shown in figure 9. Comparing this with the results of the T-shaped DQD (figure 6), it is found that for the case $\Delta_1 = \Delta_2$ ($\neq 0$), the Fano factor is 1 for any value of $W$ at small voltage (figure 9(b)). For other values of $\Delta_{1,2}$, there is no qualitative difference between the T-shaped DQD and a parallel DQD.

For the asymmetric coupling case, the behavior of the Fano factor is similar to that of the T-shaped DQD. The dependence of the Fano factor on the bias voltage is nonmonotonic, as shown in figure 10. The limiting values of the Fano factor are $F(0) = 1$ and $F(\infty) = 2\alpha^2 - 2\alpha + 1$. Thus, for the asymmetric coupling case, there is no qualitative difference between the T-shaped DQD and the type (i) parallel DQD.

Second, we consider the type (ii), i.e., $\alpha_1 = 1 - \alpha_2 = \alpha$. The transmission probability obtained by the perturbation expansion is

$$T(\omega) = \frac{(F_{\mathrm{a1},+}^2 - F_{\mathrm{a1},-}^2)D^2}{[D^2 + F_{\mathrm{a2}}^2 - F_{\mathrm{a1},+}F_{\mathrm{a1},-}]^2 + D^2(F_{\mathrm{a1},+} + F_{\mathrm{a1},-})^2}, \tag{3.14}$$

where

$$\begin{aligned} F_{\mathrm{a1},\pm} &= (\tfrac{1}{2} \pm \sqrt{\alpha(1-\alpha)})\omega(2\omega^2 - \Delta_1^2 - \Delta_2^2 - 2W^2 \\ &\quad \pm 2W(\Delta_1 + \Delta_2)), \\ F_{\mathrm{a2}} &= (\alpha - \tfrac{1}{2})(\Delta_1 - \Delta_2)(\omega^2 + \Delta_1\Delta_2 - W^2). \end{aligned} \tag{3.15}$$

For $\alpha = 0.5$, equation (3.14) agrees with equation (3.10). The dependence of the current and the Fano factor on the bias voltage is shown in figure 11. As $\alpha$ decreases, the current decreases (resulting in a negative differential conductance), and one local minimum occurs. For sufficiently small $\alpha$, the current becomes negative, and the Fano factor diverges. This is due to the breakdown of the perturbation expansion. In the limit $\alpha \to 0$, the type (ii) parallel DQD is equivalent to a serial DQD with symmetric coupling. Thus, the perturbation expansion has limitations in cases of the parallel DQD with $\alpha_1 = 1 - \alpha_2$ and the serial DQD. The breakdown of the perturbation expansion originates from the derivation of the transmission probability. The numerator of equation (3.14) is the difference of two terms; it becomes a negative value in some bias voltage ranges when $\alpha$ is small. Thus,

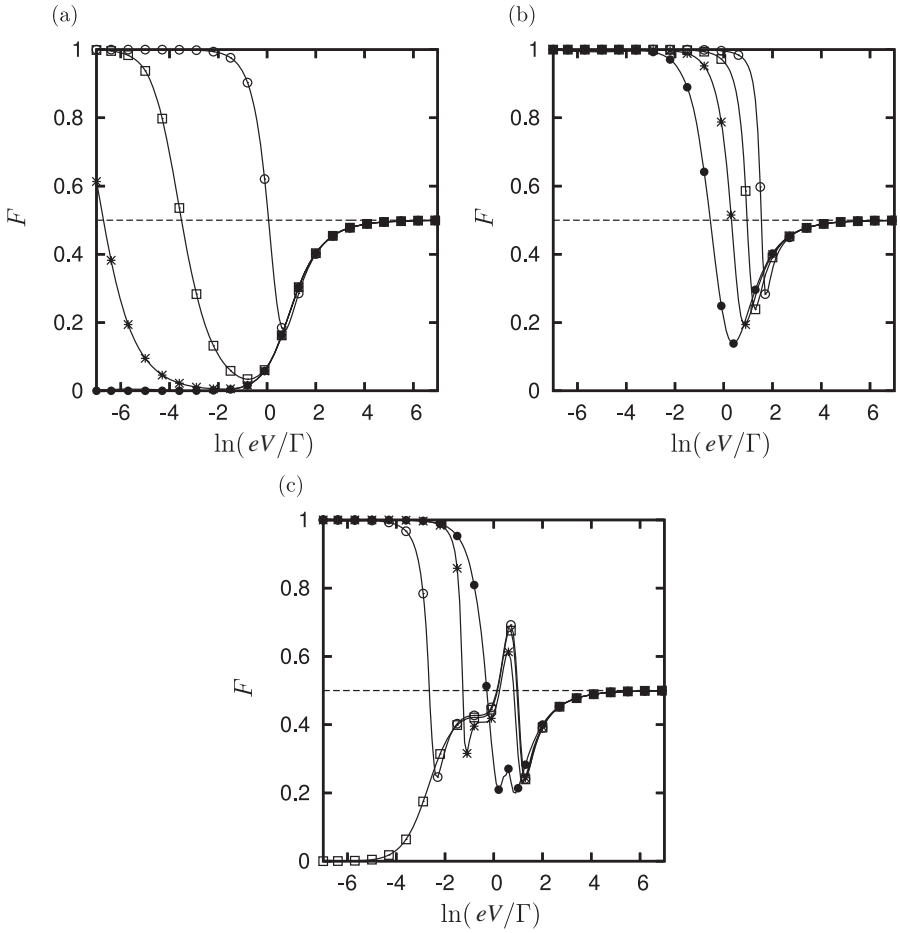


**Figure 8.** Dependence of Fano factor in type (i) parallel DQD on bias voltage for different energy levels of dots and interdot coupling. $\alpha = 0.5$. (a) $\Delta_1 = \Delta_2 = 0$. Curves denoted by ●, ∗, □, and ○ correspond to cases $W = 0.0$, 0.04, 0.2, and 1.5, respectively. (b) $\Delta_1 = \Delta_2 = 1.0$. Curves denoted by ●, ∗, □, and ○ correspond to cases $W = 0.0$, 0.8, 2.0, and 4.0, respectively. (c) $\Delta_1 = 1.0$, and $\Delta_2 = 2.0$. Curves denoted by ●, ∗, □, and ○ correspond to cases $W = 0.0$, 1.1, $\sqrt{2.0}$, and 1.5, respectively.

the second order perturbation expansion cannot be used to determine the correct behavior of a type (ii) parallel DQD when $\alpha$ is small.

Here, we present a short summary of the behavior of the Fano factor in T-shaped and type (i) parallel DQDs. There are two noteworthy features. The first feature is that the shot noise is sub-Poissonian, and $F(0)$ for $\alpha = 0.5$ is either 0 or 1 depending on the parameters $\Delta_{1,2}$ and $W$. We have found that $F(0) = 1$ for $\alpha \neq 0.5$. On the other hand, $F(\infty)$ is independent of these parameters, $F(\infty) = 2\alpha^2 - 2\alpha + 1$. This limiting value is same as that in the case of a SQD, so that the behavior of the Fano factor at large bias voltage is essentially same as that in a SQD. The second feature is that the nonmonotonic behavior of the Fano factor results from the interdot coupling; three local extrema can occur in the Fano factor. The interdot coupling causes the mixing of bare energy levels of dots to form effective energy levels of dots. The transmission probability has a complex dependence on $\Delta_{1,2}$ and $W$, and there can be three solutions for $F(V^*) = (1 - T(eV^*))$ in the range $V^* > 0$. This leads to three local extrema in the Fano factor. Thus, the behavior of the Fano factor in an intermediate voltage range is different from that in a SQD.

Let us discuss the influence of the Klein factor on our results. In the bosonization and refermionization processes, we neglected the Klein factor, so that the Fermi statistics of electrons does not hold. By using the renormalization group method, it was shown that the current does not flow when the Klein factor is considered for an asymmetric ($\alpha \neq 1/2$) type (i) parallel DQD with $W = 0$ [38]. On the other hand, for the symmetric coupling case ($\alpha = 1/2$), the model flows to an intermediate fixed point $\gamma_{1,\mathrm{L}}^2 = \gamma_{2,\mathrm{L}}^2 = \gamma_{1,\mathrm{R}}^2 = \gamma_{2,\mathrm{R}}^2 = 4\pi^2(1 - 1/(2g))$ ($\equiv\gamma_{\mathrm{c}}^2$). This suggests that current flows for $g > 1/2$. In this study, we chose $g = 1/2$, for which $\gamma_{\mathrm{c}} = 0$, so that the current does not flow even if the coupling is symmetric. Thus, with the Klein factor and $g = 1/2$, the current does not flow for both symmetric and asymmetric type (i) parallel DQDs. The results of this study are valid if the Fermi statistics of electrons can be neglected.

## 4. Conclusions

We studied the transmission probability and the Fano factor for T-shaped and parallel DQDs connected with two infinite LL electrodes. The original Hamiltonian was mapped to the

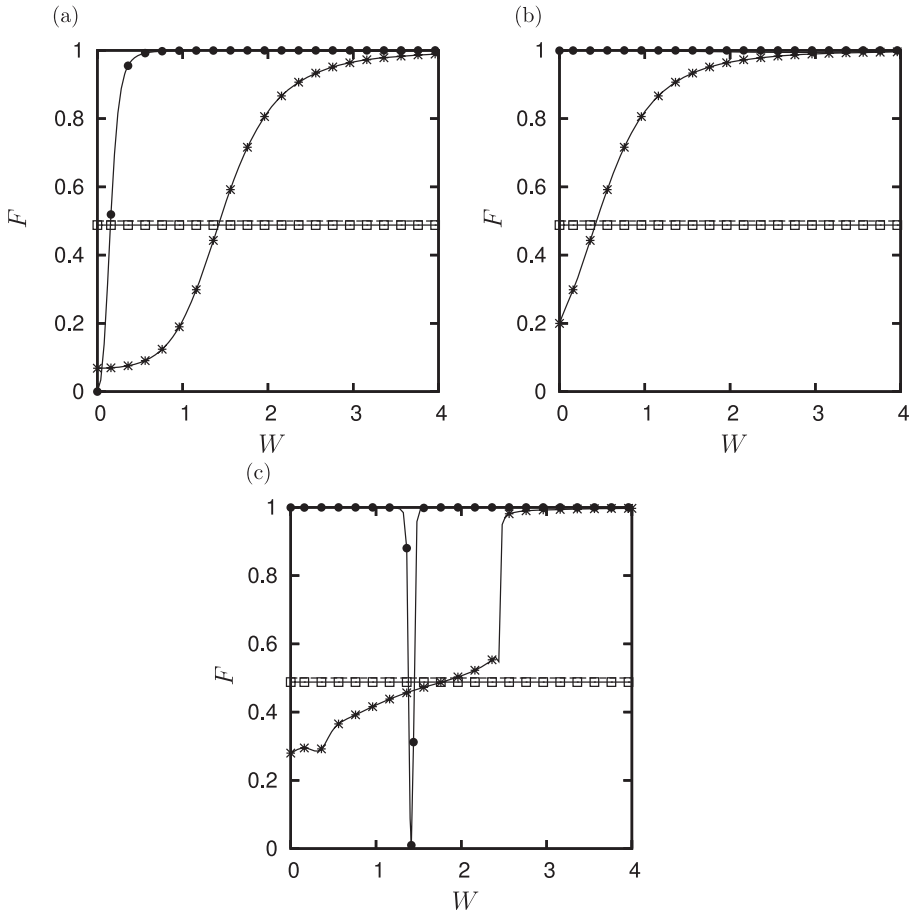


**Figure 9.** Dependence of Fano factor in type (i) parallel DQD on interdot coupling for different energy levels of dots. $\alpha = 0.5$. (a) $\Delta_1 = \Delta_2 = 0$, (b) $\Delta_1 = \Delta_2 = 1.0$, and (c) $\Delta_1 = 1.0$, and $\Delta_2 = 2.0$. Curves denoted by ●, ∗, and □ correspond to cases $\ln(eV/\Gamma) = -4.0$, 0.0, and 4.0, respectively.

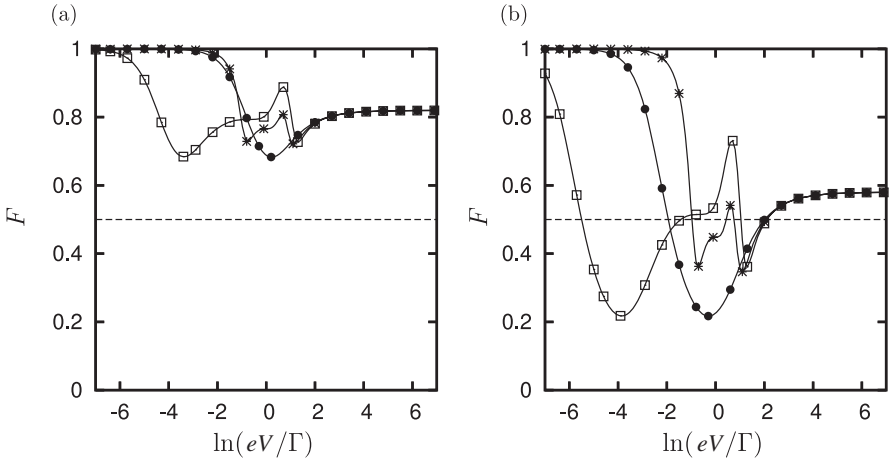


**Figure 10.** Dependence of Fano factor in type (i) parallel DQD on bias voltage for different energy levels of dots, interdot coupling, and asymmetry parameter. (a) $\alpha = 0.1$ and (b) $\alpha = 0.3$. Curves denoted by ●, ∗, and □ correspond to cases $(\Delta_1, \Delta_2, W) = (0,\ 0,\ 0)$, (2, 0, 1), and (2, 1, $\sqrt{2}$), respectively.

Kondo-type Hamiltonian at the Toulouse point; however, the Klein factor was neglected in the derivation. Consequently, the results of this study are valid if the Fermi statistics of electrons can be neglected. Applying the $S$-matrix expansion, we derived the current and the shot noise up to the second order of $\gamma_{\pm 1,2}$. In order to numerically calculate them, we derived the complete set of Green's functions by the perturbation expansion. We first verified the validity of the perturbation method for a SQD. The Fano factor in a SQD at large bias voltage does not depend on the energy level, but on the

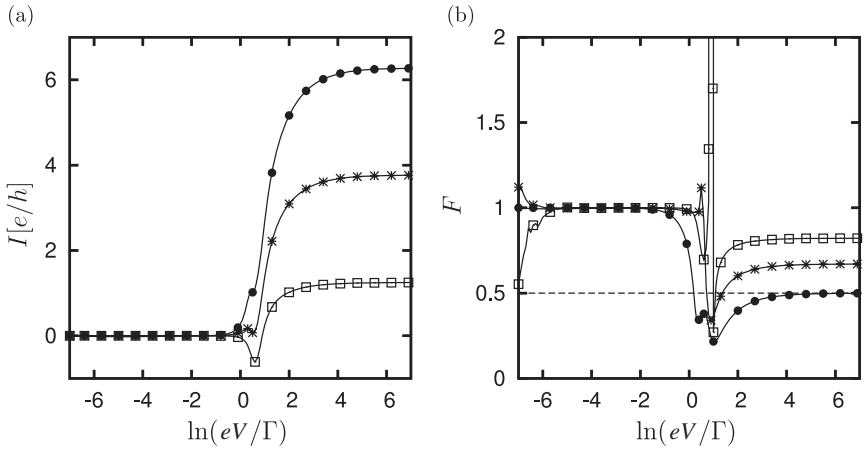


**Figure 11.** Dependence of (a) current and (b) Fano factor in type (ii) parallel DQD on bias voltage for different asymmetry parameter. $\Delta_1 = 2$, $\Delta_2 = -1$, and $W = 1$. Curves denoted by ●, ∗, and □ correspond to cases $\alpha = 0.5$, 0.1, and 0.01, respectively.

asymmetry parameter. Similarly, the Fano factor in a DQD at large bias voltage is same as that in a SQD. On the other hand, the structure of the transmission probability for a DQD has a complex dependence with energy levels and interdot coupling. When the relation $F(V^*) = (1-T(eV^*))$ $(V^* > 0)$ is satisfied self-consistently, a local extremum occurs in the Fano factor. The number of solutions corresponds to the number of local extrema in the Fano factor. Thus, the Fano factor in a DQD behaves nonmonotonically, and local minima and maxima can occur in an intermediate voltage range.

The nonmonotonic behavior of the Fano factor in a DQD connected with Fermi liquid leads under strong on-site Coulomb interactions has been studied [30–32]. In such systems, the Kondo effects, Fano interference, antiferromagnetic exchange interaction between dots, and Coulomb blockade cause the nonmonotonic behavior of the Fano factor. In contrast, although the intradot and interdot Coulomb interactions are not considered in our model, the Fano factor shows a nonmonotonic behavior when the relation $F(V^*) = (1 - T(eV^*))$ is satisfied self-consistently.

The limitations of the second order perturbation calculation for the Fano factor occur in two different stages. The first limitation occurs at a low bias voltage for a SQD and a DQD when $\alpha$ is small and $\Delta_{1,2}$ is large. The second limitation occurs in an intermediate bias voltage for a type (ii) parallel DQD and a serial DQD.

## Acknowledgments

The author would like to thank Dr Y Tokura and Dr T Kubo for their valuable discussions and comments.

## References

[1] Kane C L and Fisher M P A 1992 *Phys. Rev.* B **46** 15233
[2] Furusaki A and Nagaosa N 1993 *Phys. Rev.* B **47** 4631
[3] Bockrath M, Cobden D H, Lu J, Rinzler A G, Smalley R E, Balents L and McEuen P L 1999 *Nature* **397** 598
[4] Tans S J, Devoret M H, Dai H, Thess A, Smalley R E, Geerlings L J and Dekker C 1997 *Nature* **386** 474
[5] Postma H W C, Teepen T, Yao Z, Grifoni M and Dekker C 2001 *Science* **293** 76
[6] Nygård J, Cobden D H and Lindelof P E 2000 *Nature* **408** 342
[7] Mason N, Biercuk M J and Marcus C M 2004 *Science* **303** 655
[8] Gräber M R, Coish W A, Hoffmann C, Weiss M, Furer J, Oberholzer S, Loss D and Schönenberger C 2006 *Phys. Rev.* B **74** 075427
[9] Blanter Y M and Büttiker M 2000 *Phys. Rep.* **336** 1
[10] Onac E, Balestro F, Trauzettel B, Lodewijk C F J and Kouwenhoven L P 2006 *Phys. Rev. Lett.* **96** 026803
[11] Kim N Y, Recher P, Oliver W D, Yamamoto Y, Kong J and Dai H 2007 *Phys. Rev. Lett.* **99** 036802
[12] Wächter P, Meden V and Schönhammer K 2007 *Phys. Rev.* B **76** 125316
[13] Andergassen S, Enss T and Meden V 2006 *Phys. Rev.* B **73** 153308
[14] Furusaki A 1998 *Phys. Rev.* B **57** 7141
[15] Meden V, Enss T, Andergassen S, Metzner W and Schönhammer K 2005 *Phys. Rev.* B **71** 041302
[16] Nazarov Y V and Glazman L I 2003 *Phys. Rev. Lett.* **91** 126804
[17] Weymann I, Barnaś J and Krompiewski S 2008 *Phys. Rev.* B **78** 035422
[18] Weymann I, Barnaś J and Krompiewski S 2007 *Phys. Rev.* B **76** 155408
[19] Recher P, Kim N Y and Yamamoto Y 2006 *Phys. Rev.* B **74** 235438
[20] Dolcini F, Trauzettel B, Safi I and Grabert H 2005 *Phys. Rev.* B **71** 165309
[21] Guigou M, Popoff A, Martin T and Crépieux A 2007 *Phys. Rev.* B **76** 045104
[22] Komnik A and Gogolin A O 2003 *Phys. Rev. Lett.* **90** 246403
[23] Emery V J and Kivelson S 1992 *Phys. Rev.* B **46** 10812
[24] Schiller A and Hershfield S 1998 *Phys. Rev.* B **58** 14978
[25] Komnik A and Gogolin A O 2005 *Phys. Rev. Lett.* **94** 216601
[26] Gogolin A O and Komnik A 2006 *Phys. Rev.* B **73** 195301
[27] Schmidt T L, Gogolin A O and Komnik A 2007 *Phys. Rev.* B **75** 235105
[28] Nayak C, Fisher M P A, Ludwig A W W and Lin H H 1999 *Phys. Rev.* B **59** 15694
[29] Komnik A and Gogolin A O 2003 *Phys. Rev.* B **68** 235323
[30] López R, Aguado R and Platero G 2004 *Phys. Rev.* B **69** 235305
[31] Wu B H, Cao J C and Ahn K-H 2005 *Phys. Rev.* B **72** 165313
[32] Bodoky F, Belzig W and Bruder C 2008 *Phys. Rev.* B **77** 035302
[33] Egger R and Grabert H 1998 *Phys. Rev.* B **58** 10761

[34] Gogolin A O, Nersesyan A A and Tsvelik A M 1998 *Bosonization and Strongly Correlated Systems* (Cambridge: Cambridge University Press)
[35] Rao S and Sen D 2002 *Field Theories in Condensed Matter Physics* ed S Rao (Bristol: Institute of Physics Publishing)
[36] Voit J 1995 *Rep. Prog. Phys.* **58** 977
[37] Meir Y and Wingreen N S 1992 *Phys. Rev. Lett.* **68** 2512
[38] Rao S and Sen D 2004 *Phys. Rev.* B **70** 195115
[39] Jauho A P, Wingreen N S and Meir Y 1994 *Phys. Rev.* B **50** 5528
[40] Martin T and Landauer R 1992 *Phys. Rev.* B **45** 1742
[41] Chen L Y and Ting C S 1991 *Phys. Rev.* B **43** 4534
[42] Braggio A, Fazio R and Sassetti M 2003 *Phys. Rev.* B **67** 233308